

APPLICATION OF VOLUME OF FLUID (VOF) METHOD IN CONJUNCTION
WITH SHEAR STRESS TRANSPORT (SST) $k-\omega$ TURBULENCE CLOSURE
MODEL TO INVESTIGATE SPILLWAY FLOW

A THESIS SUBMITTED TO
THE GRADUATE SCHOOL OF NATURAL AND APPLIED SCIENCES
OF
MIDDLE EAST TECHNICAL UNIVERSITY

BY

FATIH BAYRAKDAR

IN PARTIAL FULLFILLMENT OF THE REQUIREMENTS
FOR
THE DEGREE OF MASTER OF SCIENCE
IN
CIVIL ENGINEERING

JULY 2017

Approval of the thesis:

**APPLICATION OF VOLUME OF FLUID (VOF) METHOD IN
CONJUNCTION WITH SHEAR STRESS TRANSPORT (SST) $k-\omega$
TURBULENCE CLOSURE MODEL TO INVESTIGATE SPILLWAY FLOW**

submitted by **FATİH BAYRAKDAR** in partial fulfillment of the requirements for
the degree of **Master Science in Civil Engineering Department, Middle East
Technical University** by,

Prof. Dr. Gülbin Dural Ünver
Dean, Graduate School of **Natural and Applied Sciences** _____

Prof. Dr. İsmail Özgür Yaman
Head of Department, **Civil Engineering** _____

Asst. Prof. Dr. Talia Ekin Tokyay Sinha
Supervisor, **Civil Engineering Dept., METU** _____

Examining Committee Members

Prof. Dr. Burcu Altan Sakarya
Civil Engineering Dept., METU _____

Asst. Prof. Dr. Talia Ekin Tokyay Sinha
Civil Engineering Dept., METU _____

Asst. Prof. Dr. Cüneyt Baykal
Civil Engineering Dept., METU _____

Asst. Prof. Dr. Melih Çalamak
Civil Engineering Dept., TED University _____

Asst. Prof. Dr. Önder Koçyiğit
Civil Engineering Dept., Gazi University _____

Date: 11.07.2017

I hereby declare that all information in this document has been obtained and presented in accordance with academic rules and ethical conduct. I also declare that, as required by these rules and conduct, I have fully cited and referenced all material and results that are not original to this work.

Name, Last name: FATİH BAYRAKDAR

Signature:

ABSTRACT

APPLICATION OF VOLUME OF FLUID (VOF) METHOD IN CONJUNCTION WITH SHEAR STRESS TRANSPORT (SST) $k-\omega$ TURBULENCE CLOSURE MODEL TO INVESTIGATE SPILLWAY FLOW

Bayrakdar, Fatih

M.Sc., Department of Civil Engineering

Thesis Supervisor: Asst. Prof. Dr. Talia Ekin Tokyay Sinha

July 2017, 74 pages

Hydraulic engineers often require to assess the reasons and consequences of interaction of flow with structures. Computational Fluid Dynamics (CFD) became a useful tool in this regard in recent years as it provides ample amount of information both on flow and its interaction with its surrounding. To this end, flows over a spillway are investigated. The computational domain for the flow over a spillway is based on the study by Dargahi (2006). Numerical results are compared to previous experimental ones. In the study, SST $k-\omega$ Model is considered for turbulence closure. The free surface of these flows is simulated using Volume of Fluid (VOF) approach. The effect of spillway roughness, scale of the model, and the downstream conditions are discussed for a single spillway structure. The scale effects have shown that cavitation related studies should be carried using prototype scales in numerical simulation of spillway flows. If the roughness is accounted only as a constant in governing equations in Reynolds-Averaged-Navier-Stokes (RANS) simulations,

current study shows that its effect may not be captured pronouncedly. Downstream conditions imposed in the model could produce simple hydraulic jump conditions. In these cases, air-entrainment due to jump is calculated based on aerated fluid volume.

Keywords: Spillway, Volume of Fluid, Fluent, Scale Effect, Cavitation

ÖZ

SIVI HACMİ YAKLAŞIMI (SHY) METODUNUN KAYMA GERİLMESİ AKTARMALI (KGA) $k-\omega$ TÜRBULANS TAMAMLAMA MODELİ İLE BİRLİKTE UYGULANARAK DOLUSAVAK ÜZERİNDEKİ AKIŞIN ARAŞTIRILMASI

Bayrakdar, Fatih

Yüksek Lisans, İnşaat Mühendisliği Bölümü

Tez Yöneticisi: Yrd. Doç. Dr. Talia Ekin Tokyay Sinha

Temmuz 2017, 74 sayfa

Hidrolik mühendisleri sık sık yapıların akış ile etkileşiminin neden ve sonuçlarını değerlendirmek zorundadırlar. Hesaplamalı Akışkanlar Dinamiği (HAD), akış ve onun çevresi ile etkileşimi hakkında bol miktarda bilgi sağladığından son yıllarda bu konunun araştırılmasında yararlı bir araç haline gelmiştir. Bu amaçla, bir dolusavak üzerindeki akış araştırılmıştır. Dolu savak üzerindeki akışın sayısal akı alanı Dargahi (2006) tarafından yapılan çalışmalara dayanmaktadır. Sayısal sonuçlar önceki deneysel sonuçlarla karşılaştırılmıştır. Çalışmada, Kayma Gerilmesi Aktarmalı (KGA) $k-\omega$ Modeli yöntemi türbülans yaklaşımı için kullanılmıştır. Bu akımların serbest yüzeyleri Sıvı Hacmi Yaklaşımı (SHY) kullanılarak modellenmiştir. Dolusavak pürüzlülüğü, model ölçeği ve mansap durumlarının etkileri tek bir dolusavak yapısı için tartışılmıştır. Ölçek etkileri göstermiştir ki; Kaviteasyon ile alakalı çalışmalar prototip ölçekleri kullanılan dolusavak akışı nümerik simülasyonları ile yapılmalıdır. Çalışma sonuçları göstermiştir ki; yüzey pürüzlülüğü RANS simülasyonlarında sadece denklemde bir sabit olarak hesaba alındığında göze çarpan bir etkisi olmamaktadır.

Modele empoze edilen mansap durumları hidrolik sıçrama oluşturabilmektedir. Bu durumlarda sıçramaya bađlı hava sürüklemesi havalanmış sıvı hacmi ile hesaplanmaktadır.

Anahtar Kelimeler: Dolusavak, Sıvı hacmi yaklaşımı, Fluent, Ölçek etkisi, Kaviteasyon

ACKNOWLEDGEMENTS

I would like to thank my advisor Asst. Prof. Dr. Talia Ekin Tokyay Sinha who has supported me for my graduate studies. I also would like to thank my wife Ayşe for her patience and great support.

TABLE OF CONTENTS

ABSTRACT	v
ÖZ.....	vii
ACKNOWLEDGEMENTS	ix
TABLE OF CONTENTS	x
LIST OF FIGURES.....	xii
LIST OF TABLES	xv
CHAPTERS	
1. INTRODUCTION.....	1
2. LITERATURE REVIEW	5
3. FLOW DOMAIN, COMPUTATIONAL GRID AND BOUNDARY CONDITIONS.....	19
3.1 Introduction.....	19
3.2 Simulation Setup.....	19
3.2.1 Computational Domain, Grid and Boundary Conditions.....	19
3.2.1.1 No Jump Cases	24
3.2.1.2 Jump Cases	24
3.2.2 Governing Equations.....	24
3.2.3 SST k- ω Model.....	26
3.2.3.1 Transport Equations for SST k- ω Model	27
3.2.3.2 Wall Boundary Conditions	28
3.2.4 Roughness Effect.....	29
3.2.5 Volume of Fluid (VOF) Model	30
3.2.6 Dimensional Analysis	31

3.2.7 Fluent Setup	33
4. RESULTS AND DISCUSSION	37
4.1 Flow over Spillways under Several Downstream Conditions	37
4.1.1 Effect of Roughness on Free Surface.....	39
4.1.2 Scaling Effect and Cavitation Index Calculations	45
4.1.3 Development of Simple Hydraulic Jump at the Apron for Various Discharge and Downstream Boundary Conditions	51
4.1.4 Air Entrainment as a Consequence of Jump	55
4.1.4 Jump Types and Lengths.....	65
5. CONCLUSION AND FUTURE WORK.....	69
5.1 Conclusion	69
5.2 Future Work.....	69
REFERENCES.....	71

LIST OF FIGURES

FIGURES

Figure 1.1 Butterley Spillway – West Yorkshire, UK (Web-1, 2012).....	2
Figure 1.2 Cefni Dam – Anglesey,UK (Web-2, 2013)	2
Figure 1.3 Elkwater Fork Dam– West Virginia, USA (Web-3, 2011).....	3
Figure 2.1 Relative percent errors in Discharge Using Physical Model as Basis (Savage and Johnson, 2001).....	7
Figure 2.2 Flow visualization of north spillway at design flow. (Gessler, 2005)	8
Figure 2.3 Comparison of transverse water surface profile at the crest (Lesleighter <i>et al.</i> , 2008)	10
Figure 2.4 Comparison of water surface elevations between CFD and physical models. The crest elevations of the existing and auxiliary spillways are also shown. (Li <i>et al.</i> , 2011).....	12
Figure 2.5 Spillway geometry of study of (Mu <i>et al.</i> 2012).....	14
Figure 2.6 Comparison of computation and measurement of surface elevation (Mu <i>et al.</i> 2012).....	14
Figure 2.7 Comparison of computation and measurement of pressure on the bottom. (Mu <i>et al.</i> , 2012).....	15
Figure 2.8 Comparison of computed and measured average flow velocity for Q = 2500 m ³ /s. (Fadaei-Kermani and Barani, 2014).....	16
Figure 2.9 a) Flow over the spillway at the laboratory and b) flow visualization over the spillway using RANS modeling. (Herrera-Granados and Kostecki, 2016)	17
Figure3.3 Toe details (USACE, 1992)	22
Figure 3.4 Volume Fraction of water for case H9J	31
Figure 3.5 Scale effect simulation matrix	33

Figure 3.6 FLUENT Launcher Screen	34
Figure 3.7 General Settings.....	35
Figure 3.8 Run Calculation setting	36
Figure 4.1 Sketch of the domain that shows the location of the numerical measurements upstream over the crest and at the toe of the spillway.	38
Figure 4.2 Water surface profile for H9 case. Numerical and experimental (Dargahi, 2006) results are compared.	38
Figure 4.3 Shape of free surface over the spillway. The free surface is assumed to pass through $\alpha=0.5$	39
Figure 4.4 Free surface profiles of L1 and L4 (top), and D5 and D8 (bottom).	40
Figure 4.5 Near-wall change in velocity distribution for low flow cases over the spillway.	41
Figure 4.6 Near-wall change in velocity distribution for high flow cases over the spillway.	42
Figure 4.7 Velocity profiles at the toe for L, D and H cases after the rough spillway.	43
Figure 4.8 Velocity comparisons between D6 x 25 and P25 cases.....	45
Figure 4.9 Velocity comparisons between D6 x 50 and P50 cases.....	46
Figure 4.10 Cavitation index comparisons between model (a) and prototype cases (b) and (c).....	48
Figure 4.11 Simple hydraulic jump in low discharge case, L1J	51
Figure 4.12 Simple hydraulic jump in design discharge case, D5J	52
Figure 4.13 Formation of the jump at the downstream of the apron for the design discharge case, D5J, and its evolution towards spillway	53
Figure 4.14 Free surface oscillations after jump settles at its position at the toe of the spillway for D5J	53
Figure 4.15 Simple hydraulic jump in high discharge case, H9J.....	54
Figure 4.16 The formation and evolution of a choked jump for high discharge case, H9J2	55
Figure 4.17 Air entrainment evolution with respect to time for L1J Case.....	56

Figure 4.18 Air entrainment evolution at several time instants for L1J Case (a-h). ..	58
Figure 4.19 Air entrainment evolution at several time instants for L1J Case (i-k)....	59
Figure 4.20 Air entrainment evolution with respect to time for D5J Case	59
Figure 4.21 Air entrainment evolution at several time instants for D5J Case	60
Figure 4.22 Air entrainment evolution with respect to time for H9J Case	61
Figure 4.23 Air entrainment evolution at several time instants for H9J Case (a-d)...	61
Figure 4.24 Air entrainment evolution at several time instants for H9J Case (e-i)....	62
Figure 4.25 Air entrainment evolution with respect to time for Q1 Case	63
Figure 4.26 Air entrainment evolution at several time instants for Q1 Case (a-g)	64
Figure 4.27 Air entrainment evolution at several time instants for Q1 Case (h-g)....	65
Figure 4.28 Length of jump in sloping channels as a function of F_1 and S_0 (Bakhmeteff and Matzke, 1936).....	66
Figure 4.29 Length in terms of sequent depth y_2 of jumps in horizontal channels (USBR, 1955).....	66

LIST OF TABLES

TABLES

Table 2.1 Comparison of discharge and average velocity (Ho <i>et al.</i> , 2001).....	6
Table 3.1 Simulation matrix.....	20
Table 3.2. Simulation Matrix including roughness parameters and downstream flow depth.....	23
Table 3.3 Additional jump cases.....	23
Table 3.4 y^+ values for several computational grids.....	29
Table 4.1 Comparison of values obtained from CFD, study of Dargahi (2006) and calculation for L cases.....	43
Table 4.2 Comparison of values obtained from CFD, study of Dargahi (2006) and calculation for D cases.....	43
Table 4.3 Comparison of values obtained from CFD, study of Dargahi and calculation for H cases.....	44
Table 4.4 Discharge, inlet area and average velocity of D6, P25 and P50 cases.....	47
Table 4.5 Comparison of average velocity values obtained from CFD and at $y=0.2h$ and $y=0.8h$	50
Table 4.6 Values and jump types of jump cases.....	67
Table 4.7 Comparison of jump lengths obtained by CFD, Bakhmeteff and Matzke (1936), USBR (1955) and USACE (1992).....	67

CHAPTER 1

INTRODUCTION

Spillways are one of the most important structures of dams. During the design and later in maintenance stages, model studies of these structures are common practice. In the past, experimental modeling was widely used. Nowadays, experiments are often accompanied by numerical modeling of these and many other hydraulic structures. Spillways frequently experience lifting pressure and cavitation problems. These problems may cause vast economical losses, even collapse of the dam structure and furthermore casualties. In order to prevent these losses, spillways must be designed and built carefully. Surface roughness is also an important parameter in design of hydraulic structures. Roughness may have significant effect on pressure, discharge and velocity profiles. Roughness may change in time as some structures might have vegetation acting as roughness on them. Some examples are given in Figures 1.1, 1.2 and 1.3. Therefore, how roughness is handled in numerical studies is an important research area in hydraulic engineering.



Figure 1.1 Butterley Spillway – West Yorkshire, UK (Web-1, 2012)



Figure 1.2 Cefni Dam – Anglesey, UK (Web-2, 2013)



Figure 1.3 Elkwater Fork Dam– West Virginia, USA (Web-3, 2011)

Another important feature of spillway flow is the formation of energy dissipating hydraulic jump at the stilling basin of the structure. Downstream conditions play key-role in formation of jump.

Physical models are used in laboratories in the design stage of spillway structures. However, these studies are expensive and time-consuming. Furthermore, there can be many problems associated with scaling effects. But in recent years, Computational Fluid Dynamics (CFD) codes provides efficient solutions to investigate and design hydraulic structures with less time and expense thanks to vast technological advances in computational science.

CFD is a branch of fluid dynamics, which uses governing equations and computer power to analyze and solve fluid flow problems. One can easily calculate fluid forces and comprehend the influence of fluid on hydraulic structures. CFD codes solve

complex equations and algorithms with reasonable assumptions and additional equations. However, it should be noted that despite all these advantages, CFD does not yield 100 percent reliable results. Before performing the simulation, all available input data should be checked carefully then suitable mathematical models and equations should be selected precisely according to the case. If CFD is used in conjunction with laboratory investigations it would help to overcome delays and redundant expense.

In this study, spillway flow is analyzed with different discharge, surface roughness height and length scales via Computational Fluid Dynamics (CFD). For this purposes 21 scenarios are simulated using FLUENT software. Main purpose of the study is to investigate the performance of the CFD under different spillway flow conditions and compare the numerical results with previous studies.

The spillway used in this modeling study is based on the one used by Dargahi (2006). The crest height is 0.2 m, width of the channel is 0.403 m, length is 4 m and the depth is 0.6 m. These values are based on physical experiments done by Dargahi (2006). The scale is therefore quite small in comparison to any prototype scale.

In Chapter 2, relevant studies from literature are summarized. In Chapter 3, model parameters, governing equations, computational grid and boundary conditions are briefly explained. Simulation setup is also given in this chapter. In Chapter 4, results obtained are discussed. Some comparisons made with other studies are also in this chapter. In last chapter, conclusion of the study and some future recommendations are given.

CHAPTER 2

LITERATURE REVIEW

Computational fluid dynamics (CFD) have been increasingly used in investigating flow over spillways because of the economical concerns and the time consuming experimental studies. After the validation of numerical model with physical model tests, it can be used as a design tool. In the design of overflow spillways, information regarding the hydraulics of the flow over and around the structure is of interest. Obtaining discharge-rating curves in the design stage of these structures is quite important in order to safely pass the design flood at the prescribed forebay level. In this chapter some recent numerical studies on spillway and other hydraulic structures in the literature are summarized.

Ho *et al.* (2001) investigated the spillway behavior under rising flood levels two- and three-dimensionally with CFD Techniques. The CFD code FLOW-3D was used in the study. The depth and the average velocity over the crest were retrieved from the numerical simulation of flow over a spillway with existing head to design head ratios (H_c/H_d) of 1.33, 1 and 0.5. Their results, which have been given in Table 2.1, were in good agreement with the values obtained using empirical equations. In this table Q is the discharge, L is the effective length of spillway, y_c is the depth of the flow over the crest and V is the average velocity at the crest

Table 2.1 Comparison of discharge and average velocity (Ho *et al.*, 2001)

H_c/H_d	Empirical Results			Computed Results			
	Q/L ($m^3/s/m$)	y_c (m)	V (m/s)	Q/L ($m^3/s/m$)	Diff. (%)	V (m/s)	Diff. (%)
1.33	95.6	10.0	9.6	112.3	17	10.9	14
1	61.0	7.5	8.1	70.7	16	9.4	16
0.5	20.9	3.8	5.5	22.9	10	6.1	12

They also compared the pressure distributions over the structure for different heads obtained via CFD with the ones obtained through physical models. The results validated against United States Army Corps of Engineers (USACE) and Waterways Experiment Station (WES).

Savage and Johnson (2001) completed a study to compare flow parameters over a standard ogee-crested spillway using a physical model, numerical model, and existing literature. They also employed FLOW-3D as the numerical tool of their study. Data interpolated from U.S. Bureau of Reclamation (USBR) and U.S. Army Corps of Engineers (USACE) design monographs provided discharge and pressure data from the literature. Non-dimensional discharge curves were used to compare the results obtained from different methods. Pressures were compared at low, mid, and high flow conditions. Their physical and numerical findings are in reasonably good agreement for both pressures and discharges. Relative errors based on physical model of the study of Savage and Johnson (2001) are given in Figure 2.1.

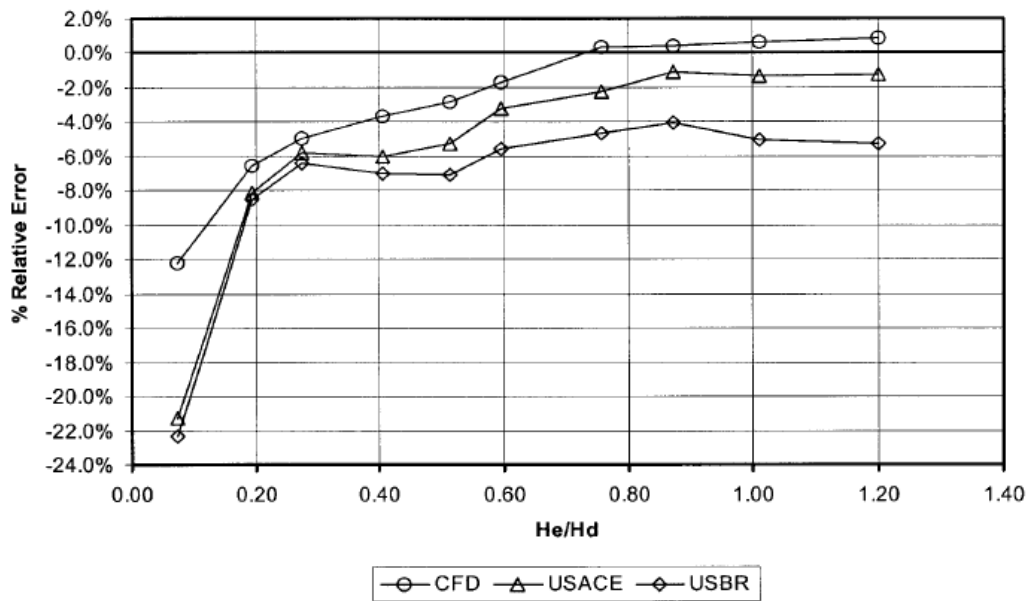


Figure 2.1 Relative percent errors in Discharge Using Physical Model as Basis (Savage and Johnson, 2001)

Bouhadji (2004) modeled numerically the flow over a spillway using CFX software, and compared the results with the USACE experimental data. In the study of Bouhadji (2004), the shear stress transport (SST) based $k-\omega$ turbulence model was used for turbulence modeling and homogeneous model was used for simulating the multiphase fluid streams. The results showed very good agreement with the experimental data.

Dargahi (2004) applied a three-dimensional flow model that uses the RNG (renormalized group theory model) $k-\epsilon$ turbulence model and a non-equilibrium wall function to the River Klarälven in the southwest part of Sweden to study the nature of the flow in the river bifurcation and to investigate the short-term sediment transport patterns in the river. FLUENT was used in the study. Numerically obtained length of surface flow separation zones were compared to the field observations. Numerical model results and field observations were compared and it was found that difference was in the range of 7-12%.

Gessler (2005) tested a three dimensional CFD model for a portion of a lake and two spillways by FLOW-3D. Results were validated against a 1960 model study, which has been made by Alden Research Laboratory, Inc. The rating curves obtained through physical model and CFD study are compared. An example of flow visualization is given in Figure 2.2. Under various flow conditions results closely matched with the observations from physical model.

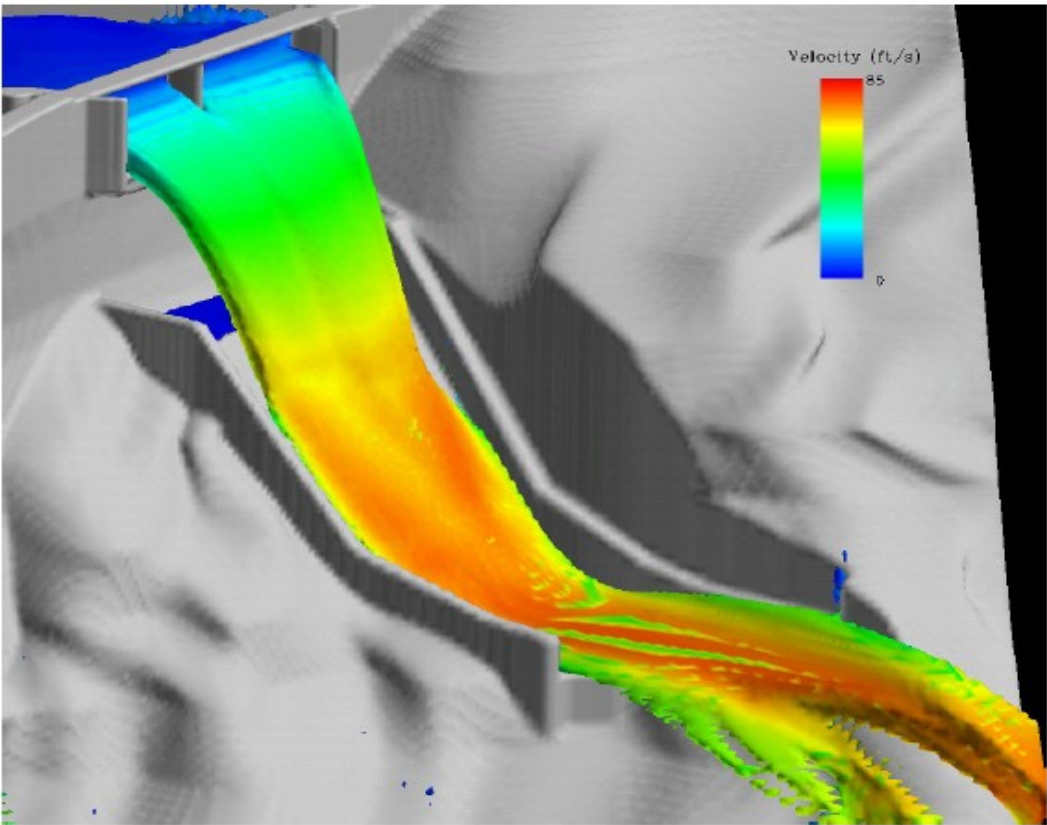


Figure 2.2 Flow visualization of north spillway at design flow. (Gessler, 2005)

Kim and Park (2005) investigated flow characteristics such as flowrate, water surface profiles, crest pressure on the spillway, and vertical velocity and pressure profiles under the consideration of model scale, prototype scale and surface roughness effects using FLOW-3D. Two-equation RNG model was used for turbulence closure. Three different model scales 1/50, 1/100 and 1/200 are considered in their study and the

results were compared to the prototype scale under three different ratios of H_e/H_d that are 1.33, 1.0 and 0.5. In the study, it is concluded that the discharge flowrate decreases slightly as surface roughness height and the length scale of the model to the prototype ratio increase. The pressures on the spillway crest are also observed to be somewhat different with a change of the surface roughness and model scale. Maximum velocity at any section is slightly decreasing as the surface roughness and the length scale ratio increase.

Dargahi (2006) used FLUENT software to analyze flow over spillways. The model spillway was designed according to the Waterway Experiment Station (WES) standard (USACE,1952) for a design head of $H_d=0.1$ m. Detailed measurements of water surface profiles and velocity distributions normal to the streamlines were made at three different operating heads of $0.5H_d$, $1.0H_d$, and $1.15H_d$. To investigate the influence of a low Reynolds number, additional water surface measurements were taken for $H_0=0.1H_d$. For turbulence closure, several methods used and compared. He obtained the best agreement with experiments using RNG model with the non-equilibrium wall function. The water surface profiles and the discharge coefficients for a laboratory spillway were predicted within an accuracy range of 1.5–2.9%. The simulations were found to be sensitive to the choice of the wall function, grid spacing, and Reynolds number.

Chanel and Doering (2007) discussed three-dimensional numerical modeling of three different spillway configurations used by Manitoba Hydro at Wuskwatim, Limestone, and Conawapa using FLOW-3D and compared the predicted rating curves, pressures, and water surface elevations to corresponding values from physical model experiments. RNG turbulence model was used in this study. The numerical model results were generally in agreement with physical model data, however, the relative differences in discharges were found to have a P/H_d dependency. In a follow-up study, Chanel and Doering (2008) discussed effect of different mesh resolutions, turbulence options and numerical options for all three spillways considered in Chanel and Doering (2007).

Lesleighter *et al.* (2008) used CFD for the hydraulics investigations required for the spillway upgrade works for Lake Manchester Dam, which is a 38 m high concrete gravity structure, constructed between 1912 and 1916. The spillway has experienced erosion, most notably during a flood in the 1930s in which the non-overflow section of dam was overtopped by 0.6 m. The erosion in the spillway resulted in a hole around 30 m deep. FLOW-3D software was used to determine flow velocity, bottom pressure, and water surface profiles in the approach channel, chute and plunge pool, with a particular focus on the approach flow conditions and spillway geometry effects. A series of analyses that considered four configurations for approach geometry at the Probable Maximum Flood discharge were performed. Figure 2.3 shows some of the results of study of Lesleighter *et al.* (2008).

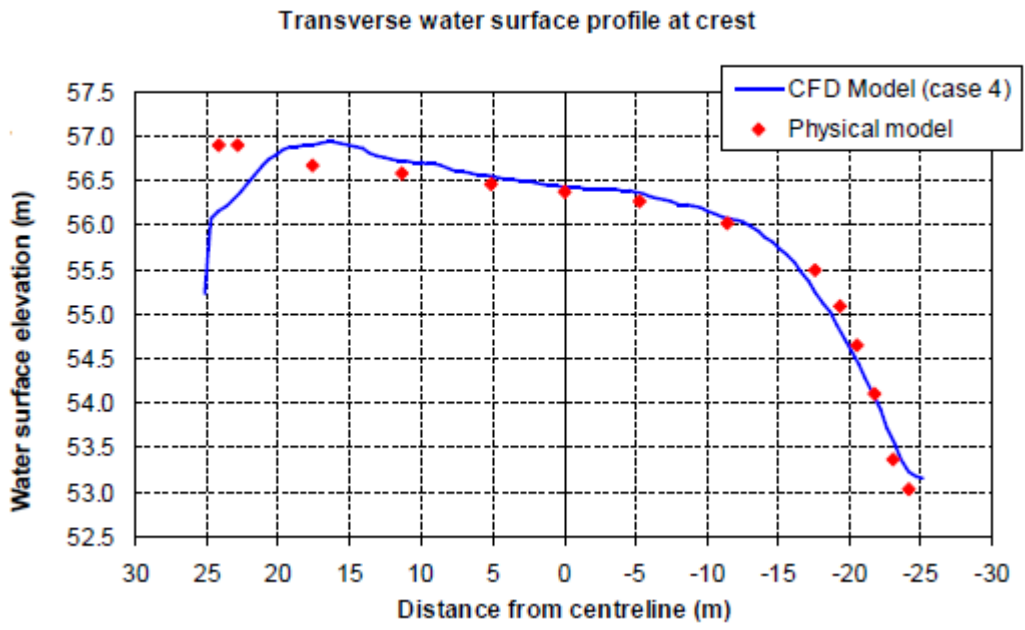


Figure 2.3 Comparison of transverse water surface profile at the crest. (Lesleighter *et al.*, 2008)

Aydin and Ozturk (2009) developed a 3D model of a spillway aerator, and compared their results to the results obtained through a physical model and the results obtained from empirical equations. FLUENT was used in the study. The four different

turbulence closure models $k-\varepsilon$, RNG $k-\varepsilon$, $k-\omega$, and Reynolds Stress Turbulence Model (RSM) were tested. The algebraic slip mixture (ASM) model was used to determine the free surface. The results through simulations agreed reasonably with prototype data but were not consistent with physical model data because of scale effects.

Akoz *et al.* (2009) conducted laboratory experiments to measure the velocities of 2D turbulent open channel flow upstream of a vertical sluice gate. Sensitivity of the numerical results to the selection of the mesh and the turbulence closure was discussed in their study.

Sung-Duk *et al.* (2010) reviewed the applicability of CFD model to simulate flow on the spillway. The study uses numerical methods based on the disadvantages of the hydraulic modeling such as scaling effects and high costs. The Karian Dam in Indonesia was selected as the study site. To analyze the flow, FLOW-3D software was used in this study. The flow stability in approach channel was investigated with the initial plan design, and results showed that the flow in approach is unstable in the initial design. To improve flow stability in the spillway, a revised plan design was formulated. The appropriateness of the revised design was examined by a numerical modeling. The results showed that the flow in spillway is stable in the revised design.

Li *et al.* (2011) presented the results of a numerical model study of probable maximum flood (PMF) flow through a system of spillways consisting of an existing service spillway and a new auxiliary spillway. Different combinations of approach channel geometries were simulated. FLUENT software was used in the study. A standard turbulence $k-\varepsilon$ model with wall functions. Approach velocity profile is used as input in the numerical study. Water surface elevation and discharge in existing and auxiliary spillways were predicted using numerical simulations. The flow patterns are also visualized. The physical model results were compared to the CFD model results, and found to be in good agreement. The CFD model was thus validated. Figure 2.4 compares numerical results of Li *et al.* (2011) to the physical model

findings in terms of water surface elevation. At 26 different locations in the domain, the average point velocity readings are compared to the readings from the physical model. The relative percent error between the numerical and the experimental results are between 1.4 -13.8%.

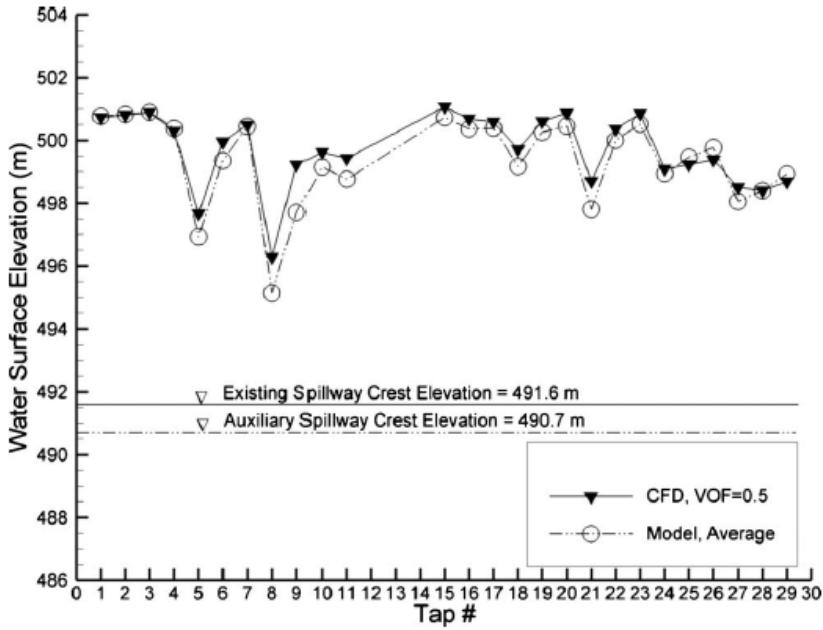


Figure 2.4 Comparison of water surface elevations between CFD and physical models. The crest elevations of the existing and auxiliary spillways are also shown. (Li *et al.*, 2011)

Morales *et al.* (2012) numerically simulated flow over an ogee shaped spillway and under a tainter gate that are planned to be constructed in Guayas Watershed in Ecuador as part of a project on a diversion dam located on the Cañar River. Interaction of flow with these structures was analyzed using FLUENT software. Among several turbulence models, $k-\omega$ model was found satisfactory. Physical model and numerical model calculations compared and numerical model was validated. Based on the numerical results, the design of the ogee shape spillway and tainter gate were found to be appropriate as the hydraulic jump occurred within the

designed basin for all simulation conditions. Reasonable agreement between the physical and the numerical results were achieved especially for flow over the spillway. This study indicated that, the discrepancies between the numerical and physical results for the flow under the gate might be due to measurement errors in the experiments.

Rahimzadeh *et al.* (2012) investigated the performance of some turbulence models to predict the hydraulic condition of flow over circular spillways. Numerical solutions compared with experimental data. The VOF method was applied to obtain the free surface in each case. FLUENT software was used to simulate flow. By comparing the 3D simulation results with the flume data obtained by other researchers, the simulation was found to produce flow over a circular spillway with sufficient accuracy by all turbulence models except the standard k- ϵ and standard k- ω models. The RSM turbulence model had the best agreement among all turbulence models with experimental data.

Mu *et al.* (2012) simulated the flow characteristics in a whole spillway based on the VOF method multidimensional two-phase flow model and standard k- ϵ method by FLUENT under the conditions of the checked flood level and a design flood level. The numerical computation results of the surface elevation, pressure and flow velocity along the spillway in two schemes fit the experimental results well, and the difference of the average velocity between calculated and experimental results was less than %6. In this study, the advanced CFD method was used to solve design problems in a practical spillway design, and the calculation results could be used as the basis of the shape optimization. The simulation domain of the study of Mu *et al.* (2012) is given in Figure 2.5. Figures 2.6 and 2.7 show the water surface level and pressure measured over the bottom of the structure, respectively. In both figures, the numerical results are observed to match well with the experimental findings.

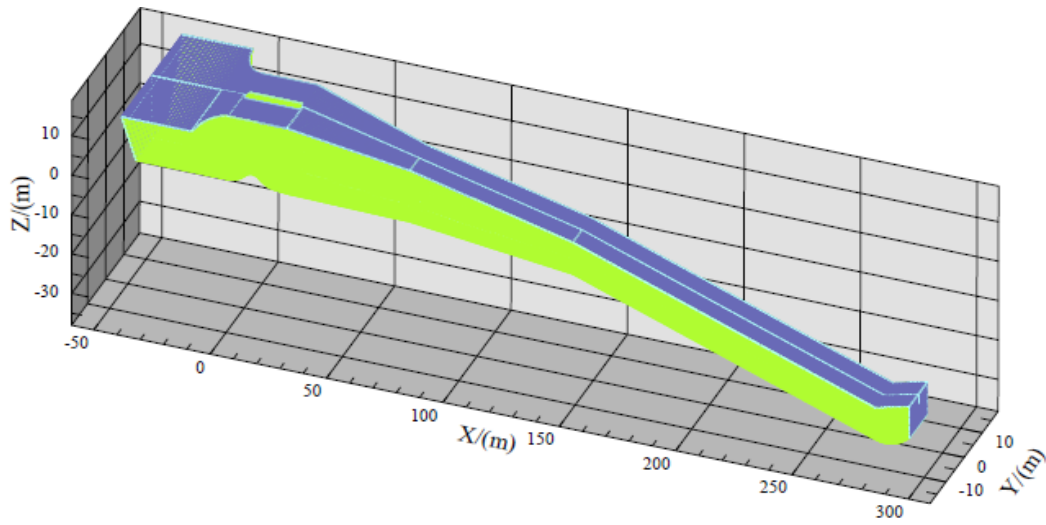


Figure 2.5 Spillway geometry of study of (Mu *et al.* 2012)

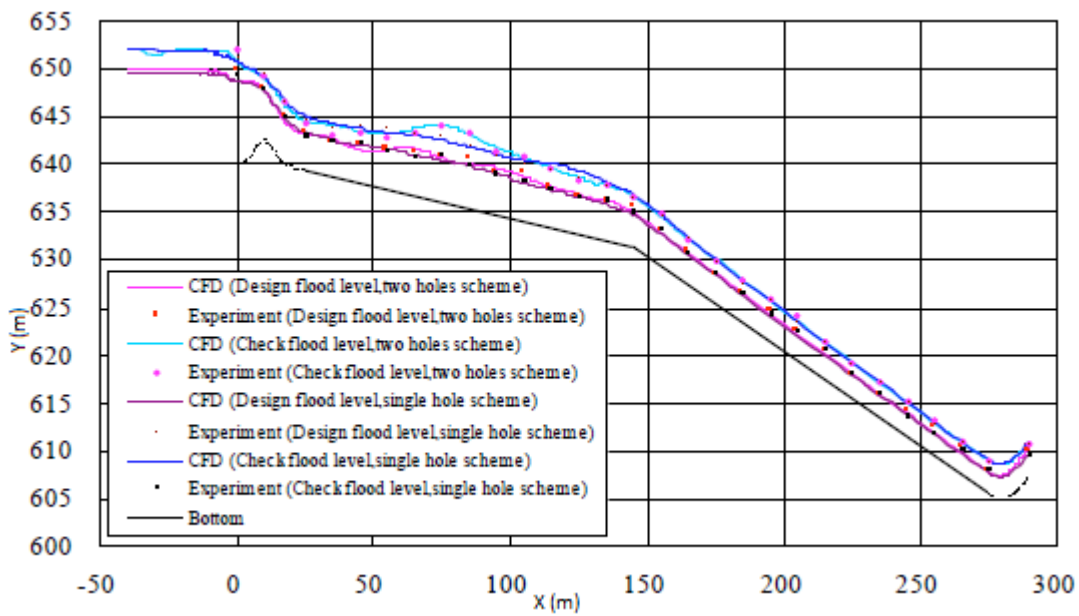


Figure 2.6 Comparison of computation and measurement of surface elevation. (Mu *et al.*, 2012)

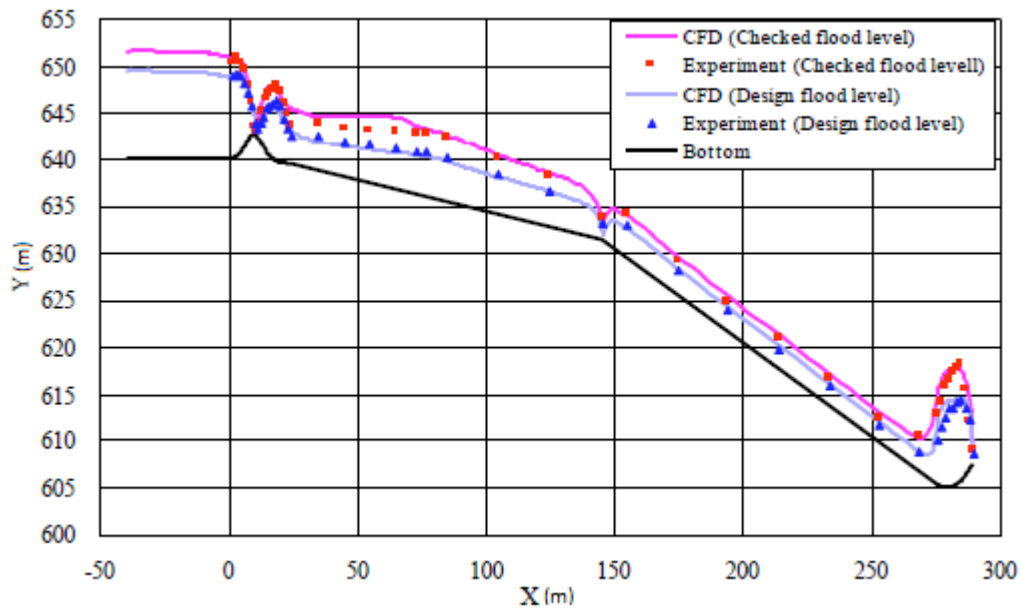


Figure 2.7 Comparison of computation and measurement of pressure on the bottom. (Mu *et al.*, 2012)

Fadaei-Kermani and Barani (2014) presented numerical simulation of flow over a chute spillway using FLOW-3D. The flow characteristics such as velocity, pressure and depth through the spillway have been calculated for four different flow rates. Since the actual flow is turbulent, the RNG turbulence model has been used for simulation. The numerically computed results of piezometric pressure and flow velocity along the spillway were compared with the results from the hydraulic model tests. The maximum difference between calculated and experimental results in average velocity values was 5.47% and in piezometric pressure values was 7.97%. The numerical results agreed well with experiments. The comparison of average velocity of computed and measured is given in Figure 2.8.

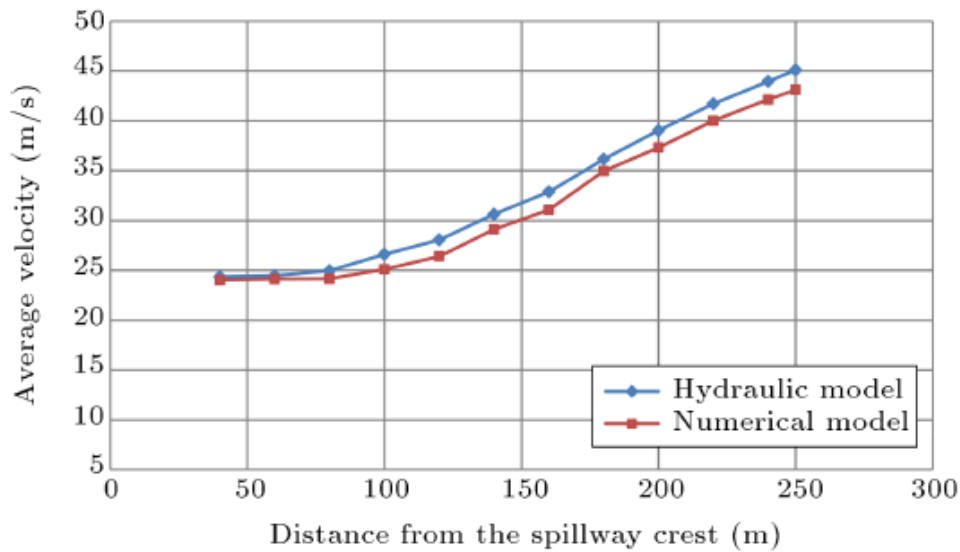


Figure 2.8 Comparison of computed and measured average flow velocity for $Q = 2500 \text{ m}^3/\text{s}$. (Fadaei-Kermani and Barani, 2014)

Parsaie, Haghiabi and Moradinejad (2015) modeled the flow pattern at the guide wall of the Kamal-Saleh Dam in Iran by FLOW-3D. The $k-\epsilon$ and RNG models have been used. The results showed that the current geometry of the left wall causes instability in the flow pattern causing secondary flow in the approach channel. This shape of guide wall reduced the performance of weir to remove the peak flood discharge.

Valero *et al.* (2016) tested both smooth chute and stepped chute configurations terminating with the USBR type III stilling basin by means of numerical modeling, allowing a qualitative comparison. Unsteady RANS (Reynolds Averaged Navier-Stokes) equations have been employed together with VOF and RNG $k-\epsilon$ for free surface tracking and turbulence modeling, respectively. Eight different Froude numbers (Fr) ranging from 3.1 to 9.5 have been analyzed for a type III basin designed for $Fr = 8$, following recent studies conducted in a physical model by Reclamation. The basin flow structure was discussed for both smooth chute and stepped chute cases. Additionally, the modeled basin has been tested for design and adverse hydraulic conditions.

Rad (2016) evaluated the use of numerical methods in the design of hydraulic structures and use a numerical model to validate the simulation of flow over three types of spillway, which are smooth spillway, various of step spillway, labyrinth spillway and side spillway. This study was to model the complex flow pattern of two-phase turbulence flow in spillways by using the numerical model. The study showed the results of correspondence between physical model and finite volume method modeled by FLOW-3D. The numerical simulation results of free surface, velocity components and air concentration in water and circumstance of air entry into the water have been compared with the experimental results.

Herrera-Granados and Kostecki (2016) applied two- and three-dimensional numerical modeling, in order to simulate water flow behavior over the new Niedów Dam in South Poland. The draining capacity of one of the flood alleviation structures (ogee weir) for exploitation and catastrophic conditions was estimated. The output of the numerical models was compared with experimental data. They used FLOW-3D to investigate a new cofferdam, which is part of the temporal reconstruction works. This additional structure was found to affect the drainage capacity of the whole low-head dam project. In Figure 2.9 the flow pattern in laboratory is compared to the one obtained through numerical simulation.

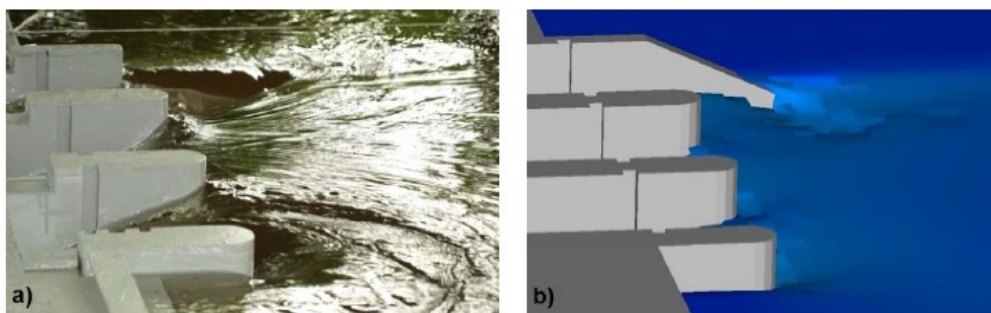


Figure 2.9 a) Flow over the spillway at the laboratory and b) flow visualization over the spillway using RANS modeling. (Herrera-Granados and Kostecki, 2016)

These previous numerical studies have shown and validated the use of numerical models in order to study free surface flows over spillway structures using VOF technique in combination with a turbulence closure model.

In literature, there are several studies, which use FLOW-3D, FLUENT and CFX to numerically investigate open-channel flow. In this study FLUENT software is selected to investigate flow over a spillway structure.

CHAPTER 3

FLOW DOMAIN, COMPUTATIONAL GRID AND BOUNDARY CONDITIONS

3.1 Introduction

In order to simulate 3D flow, a commercial CFD software FLUENT was used in this study. It can solve various types of flow including compressible and incompressible flow conditions. A RANS type model is used in the study. Free surface tracking was done using Volume of Fluid (VOF) method. This method is first introduced by Nichols and Hirt (1975) and they later made some modifications to their original approach (Hirt and Nichols, 1981). In this chapter, simulation setup in terms of computational grid and boundary conditions are discussed. The governing equations are summarized. Laboratory scale versus prototype scale simulations are also discussed in the next chapter. In this chapter, some apriori calculations for these cases are presented. Finally, a typical code setup is illustrated.

3.2 Simulation Setup

3.2.1 Computational Domain, Grid and Boundary Conditions

The flow domain is similar to the one used in the study of (Dargahi, 2006). It is a rectangular channel with 0.6m of depth, 0.403m of width and 4m of length. The crest

height P is taken as 0.2m. The flow domain is given in Figure 3.1 together with mesh details over the centerline plane, where $z=0$. The details of the crest and toe are provided in the sketch given in Figure 3.2 and Figure 3.3 respectively. Three different existing head (H_e) conditions are considered in the study. These are $H_e = 0.5H_d$, $1.0H_d$ and $1.5H_d$, where H_d is the design head. The design head for this ogee crest spillway is 0.1m. The simulation matrix is provided in Table 3.1. The discharge is calculated based on Equation (3.1), where B is the effective width of spillway and C is the discharge coefficient provided by US Army Corps of Engineers. C is a dimensional coefficient and it depends both on the ratio between existing head and design head (H_e/H_d) and on the ratio between the crest height and design head (P/H_d). In Table 3.1 the C value is referred as C_{est} as this value is estimated from design charts based on the geometry and inlet height we used in the study. C values are also calculated from simulation results later in the discussion section and compared with the experimental values. In the study, B is taken as the full width of the domain as we did not consider any pier or other type of obstruction over the spillway. In simulation matrix “L”, “D” and “H” represents Low, Design, and High discharge cases respectively.

$$Q = CBH_e^{3/2} \quad (3.1)$$

Where Q is discharge, B is effective width of spillway, C is discharge coefficient and H_e is existing head.

Table 3.1 Simulation matrix

Case	H_e/H_d	C_{est}	Q (m ³ /s)
L	0.5	2.00	0.009
D	1.0	2.15	0.027
H	1.15	2.32	0.036

The bottom and side boundaries are treated as no-slip walls, while the top boundary is treated as a symmetry surface. The inlet section is divided into two to have better

control of the elevation of the free surface of incoming flow. The outflow is treated as a regular mass outflow, which satisfies the conservation of mass conditions.

Mesh has about 580,000 hexahedral elements. Near the wall regions, the mesh size is taken around 1mm. The near wall mesh size in terms of wall units could be calculated based on an empirical formula for external flows which estimates a coefficient for the wall shear stress as $C_f = 0.058Re^{-0.2}$. This coefficient is used for finding the wall shear stress as $\tau_w = 0.5C_f\rho U^2$, where U is the average velocity. Based on the Reynolds number and average velocity of flow at the inlet section, the y^+ value near the spillway wall boundaries is estimated at around 5.3. As shown in Figure 3.1, there is a concentration of grid points around the spillway to better resolve the flow dynamics in that area. In the midstream the y^+ value is 100.

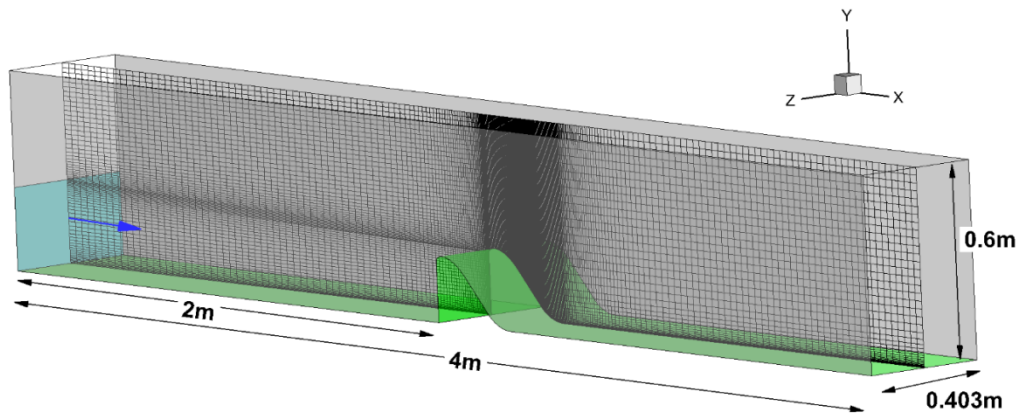


Figure 3.1 Simulation domain and the mesh details on the symmetry plane $z=0$.

The blue arrow points the flow direction. The inlet is divided into two sections to better control the air-water interface.

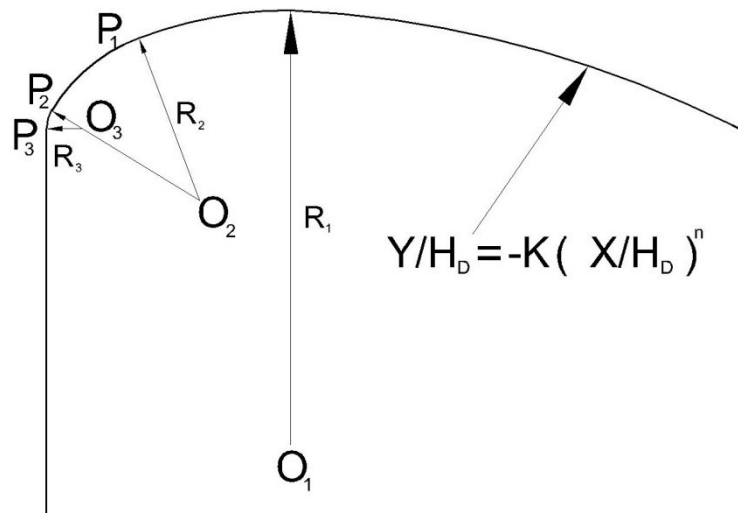


Figure 3.2 Crest details (USACE, 1992)

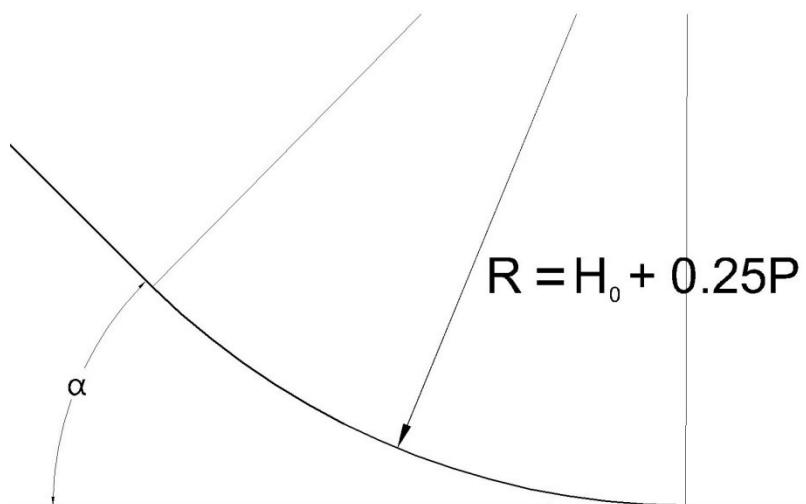


Figure 3.3 Toe details (USACE, 1992)

In order to investigate influence of the roughness, 4 different roughness heights were used. These are hydraulically smooth ($k_s=0$), smooth sheet steel ($k_s=0.07$ mm), planned wood ($k_s=0.5$ mm), and rough concrete ($k_s=2$ mm). Table 3.2 which involve the cases in present study including cases respect to different roughness heights, discharges and downstream flow depths is given below. In order to investigate jump lengths and types three additional jump cases are carried on. These cases are given in

Table 3.3 below. In these cases domain length and width are different from cases listed in Table 3.2. The crest height of the spillway for these cases are identical to the ones listed in Table 3.2. The existing head (H_e) values are taken arbitrarily to investigate the effect of higher discharge values.

Table 3.2 Simulation Matrix including roughness parameters and downstream flow depth.

Cases	H_e/H_d	Roughness Height k_s (mm)	Q (m^3/s)	Downstream Flow Depth y_2 (m)
L1	0.5	0	0.009	-
L1J	0.5	0	0.009	0.0811
L2	0.5	0.07	0.009	-
L3	0.5	0.5	0.009	-
L4	0.5	2	0.009	-
D5	1.0	0	0.027	-
D5J	1.0	0	0.027	0.1537
D6	1.0	0.07	0.027	-
D7	1.0	0.5	0.027	-
D8	1.0	2	0.027	-
H9	1.15	0	0.036	-
H9J	1.15	0	0.036	0.1728
H9J2	1.15	0	0.036	0.331
H10	1.15	0.07	0.036	-
H11	1.15	0.5	0.036	-
H12	1.15	2	0.036	-

Table 3.3 Additional jump cases

Cases	Q (m^3/s)	B (m)	Downstream Flow Depth (m)	H_e (m)
Q1	0.12	0.806	0.302	0.236
Q2	0.10	0.806	0.225	0.207
Q3	0.08	0.806	0.210	0.181

3.2.1.1 No Jump Cases

In these cases different discharge values (low, design and high) and different roughness heights that are given in Table 3.2 were considered. Combined effect of different discharges and roughness heights on flow depth and velocity profile was investigated.

3.2.1.2 Jump Cases

In these cases, downstream flow depths were obtained from Equation (3.2) for rectangular channels. Downstream flow depth is used as an input in the model and the influence of hydraulic jump on the upstream and downstream conditions and the air entrainment values at downstream of the crest are investigated.

$$\frac{y_2}{y_1} = \frac{1}{2} \left(\sqrt{1 + 8F_{r1}^2} - 1 \right) \quad (3.2)$$

Where F_{r1} is the upstream Froude number, y_1 and y_2 are upstream and downstream flow depths respectively. Here y_1 is taken from simulation results of L1, D5 and H9 as the depth of the flow after flow stabilizes downstream of the spillway over the apron. Then by using Equation (3.2), y_2 is calculated for L1J, D5J and H9J. For H9J2 case, y_2 value is taken arbitrarily to mimic flood conditions on the downstream side of the model.

3.2.2 Governing Equations

Program uses Reynolds Averaged Navier Stokes (RANS) Equations to solve complex turbulence problems conjunction with several turbulence closure models. General form of conservation of mass formulation is given in Equation (3.3), conservation of momentum is described in Equation 3.4 and where S_{ij} is the strain-rate tensor given in Equation 3.5, μ is the dynamic viscosity of the fluid.

$$\frac{\partial \rho}{\partial t} + \frac{\partial}{\partial x_i} (\rho u_i) = 0 \quad (3.3)$$

$$\rho \frac{\partial u_i}{\partial t} + \frac{\partial \rho u_i u_j}{\partial x_j} = - \frac{\partial p}{\partial x_i} + \frac{\partial}{\partial x_j} (2\mu S_{ij}) \quad (3.4)$$

$$S_{ij} = \frac{1}{2} \left(\frac{\partial u_i}{\partial x_j} + \frac{\partial u_j}{\partial x_i} \right) \quad (3.5)$$

where, ρ is the density of water, t is the time of the simulation, u_i is the velocity component, x_i is the direction considered and p is the pressure. If $i=1$, x_1 represents x -direction, whereas when $i=2$, x_2 represents y -direction, and when $i=3$, x_3 represents z -direction in Cartesian coordinate system (ANSYS FLUENT 12.0, 2009).

In order to procure calculation simplicity RANS equations are being used instead of Navier Stokes equations. In RANS equations time-averaged field variable values are being taken instead of field variables.

$$u_i = U_i + u_i' \quad (3.6)$$

$$p = P + p' \quad (3.7)$$

Capital terms are for mean and with apostrophe (') are for fluctuating in Equations 3.6 and 3.7. These equations should satisfy below conditions,

$$\bar{u}_i = U_i \quad , \quad \bar{u}_i' = 0 \quad (3.8)$$

$$\bar{p} = P \quad , \quad \bar{p}' = 0 \quad (3.9)$$

With these conditions RANS equations and strain-rate tensor S_{ij} are given below,

$$\frac{\partial U_i}{\partial x_i} = 0 \quad (3.10)$$

$$\rho \frac{\partial U_i}{\partial t} + \rho \frac{\partial}{\partial x_j} (U_i U_j) = -\frac{\partial p}{\partial x_j} + \frac{\partial}{\partial x_j} (2\mu S_{ij} - \rho \overline{u'_i u'_j}) \quad (3.11)$$

$$S_{ij} = \frac{1}{2} \left(\frac{\partial U_i}{\partial x_j} + \frac{\partial U_j}{\partial x_i} \right) \quad (3.12)$$

Final form of RANS equations after combining and substituting above equations are given below,

$$\frac{\partial U_i}{\partial t} + \frac{\partial U_i U_j}{\partial x_j} = -\frac{\partial p}{\partial x_i} + \nu \frac{\partial^2 U_i}{\partial x_i \partial x_j} - \frac{\partial \overline{u'_i u'_j}}{\partial x_j} \quad (3.13)$$

Where, ν is the kinematic viscosity.

3.2.3 SST k- ω Model

The Shear Stress Transport (SST) k- ω model is a two-equation based model which was developed by (Menter, 1994) to effectly blend the solid and accurate formulation of the k- ω model in the near wall region and the free stream independence of the k- ϵ model in the far field of flow. The SST k- ω model is similar to the standard k- ω model, but includes some refinements, which make the SST k- ω model more accurate and reliable for a wider class of flows than the standard k- ω model. Other modifications include the addition of a cross-diffusion term in the ω equation and a blending function to ensure that the model equations behave appropriately in both near-wall and far-field zones.

To solve the RANS equations some modifications and assumptions should be made. SST k- ω model fix the problems consisted from Reynolds stresses by Boussinesq approximation, which is one of the used, hypothesizes. In this approximation,

$$\tau_{ij} = -\overline{u'_i u'_j} = 2\nu_T S_{ij} - \frac{2}{3} k \delta_{ij} \quad (3.14)$$

Where, τ_{ij} is Reynolds stress tensor, ν_T is turbulence (eddy) viscosity, and δ_{ij} is Kronecker delta.

3.2.3.1 Transport Equations for SST k- ω Model

Similar to Standard k- ω model, SST k- ω model has two main equations by which one can obtain turbulence kinetic energy (k) and specific dissipation rate (ω), these are,

$$\frac{\partial}{\partial t}(\rho k) + \frac{\partial}{\partial x_i}(\rho k u_i) = \frac{\partial}{\partial x_j} \left(\Gamma_k \frac{\partial k}{\partial x_j} \right) + \widetilde{G}_k - Y_k + S_k \quad (3.15)$$

$$\frac{\partial}{\partial t}(\rho \omega u_i) + \frac{\partial}{\partial x_i}(\rho \omega u_i) = \frac{\partial}{\partial x_j} \left(\Gamma_\omega \frac{\partial \omega}{\partial x_j} \right) + G_\omega - Y_\omega + D_\omega + S_\omega \quad (3.16)$$

Where, \widetilde{G}_k is the generation of turbulence kinetic energy due to mean velocity gradients, G_ω is the generation of ω , Γ_k and Γ_ω are the effective diffusivity of k and ω respectively, Y_k and Y_ω are the dissipation of k and ω due to turbulence, D_ω is the cross diffusion term, S_k and S_ω are user defined source terms in Equations (3.17) and (3.18).

The effective diffusivities for SST k- ω are given below,

$$\Gamma_k = \mu + \frac{\mu_t}{\sigma_k} \quad , \quad \Gamma_\omega = \mu + \frac{\mu_t}{\sigma_\omega} \quad (3.17) \text{ and } (3.18)$$

Where, σ_k and σ_ω are the turbulent Prandtl numbers for k and ω respectively. μ_t is turbulent viscosity.

Turbulent Prandtl numbers are expressed using some blending functions and some empirical coefficients in the code. \widetilde{G}_k is the production of turbulence kinetic energy, G_ω is the production of ω and Y_k is the dissipation of k for incompressible flows, whereas Y_ω is the dissipation of ω for incompressible flows. More information on the turbulence model is available at (ANSYS FLUENT 12.0, 2009).

3.2.3.2 Wall Boundary Conditions

At the walls, wall functions are applied in the model. For the fine meshes, appropriate low-Reynolds-number boundary conditions will be applied. In our simulations, the computation grid is a wall-function mesh.

In FLUENT, the values of ω at the wall is specified as,

$$\omega_w = \frac{\rho (u^*)^2}{\mu} \omega^+ \quad (3.19)$$

The asymptotic value of ω^+ in the laminar sublayer is given by,

$$\omega^+ = \min \left(\omega_w^+, \frac{6}{\beta_i (y^+)^2} \right) \quad (3.20)$$

where, ω_w^+ is a function of k_s , the roughness height

In the logarithmic (or turbulent) region, the value of ω^+ is

$$\omega^+ = \frac{1}{\sqrt{\beta_\infty^*}} \frac{du_{turb}^+}{dy^+} \quad (3.21)$$

which leads to the value of ω in the wall cell as,

$$\omega = \frac{u^*}{\sqrt{\beta_\infty^*} \kappa y} \quad (3.22)$$

Here κ and β are constants.

Note that in the case of a wall cell being placed in the buffer region, FLUENT will blend ω^+ between the logarithmic and laminar sublayer values.

The wall distance y^+ is calculated in Table 3.4 given below for several computational grids that are used in the study. The Reynolds number is based on flow depth and average velocity at a section, where $x=-0.5$ m, which corresponds to a position upstream of the spillway. Therefore the Reynolds number of the incoming flow is

$Re = Vh/\nu$, where V is the average velocity at that cross-section and y is the depth of the flow at the same cross-section before the spillway. The y^+ values calculated based on the Reynolds number of the incoming flow are calculated for the mesh resolution before and after the spillway as given in the table. They are in the range of $30 < y^+ < 300$, where wall functions are applicable on the downstream side.

Table 3.4 y^+ values for several computational grids

Case	h (m)	V ₁ (m/s)	Re	C _f	U*	y ⁺	
						Before Spillway	After Spillway
L1	0.2525	0.0884	22332.51	0.0064578	0.00502	4.52	99.72
D5	0.2960	0.2263	66997.52	0.0055198	0.01189	10.70	98.71
H9	0.3159	0.2828	89330.02	0.0052976	0.01455	13.10	98.07

The size of the simulation domain is based on small-scale physical experiments. Therefore, mesh size is assumed to be sufficient for RANS-type simulations.

3.2.4 Roughness Effect

The effects of roughness are one of the most significant gradients in the flow. The effective height of the irregularities forming the roughness elements is called the “roughness height” (k_s). If the roughness height is less than a certain fraction of thickness of the laminar sublayer, the surface irregularities will be so small that all roughness elements will be entirely submerged in laminar sublayer and cannot affect the flow upon the laminar sublayer. But if roughness height is greater than a critical value, the roughness elements will extend their effects beyond the laminar sublayer and disturb the flow in the channel. (Chow, 1959)

The effect on velocity distribution is the most significant effect on the flow. Vast number of researchers investigated the effect of roughness. One of the most famous of such research is by Nikuradse (1932). He has found that velocity distributions

depends on k_s value and changes between smooth and rough surfaces for identical flows.

3.2.5 Volume of Fluid (VOF) Model

VOF is an Eulerian method that allows the user to track an interface between two or more fluids. It is often used together with Navier-Stokes equations to track air-water interface in open channel flows. A separate volume fraction equation needs to be solved by the code in order to track the evolution of the interface in time.

In the simulation air phase is represented with a volume fraction value, α of zero, while the water phase is represented with $\alpha = 1$. The volume fraction of the phase in the computational cell shows how much of that cell is occupied by that phase. If a computational cell purely consists of water, then it will have the value for variable α as 1. If the cell has an α value between 0 and 1, then this cell must have some connection with the interface. All the other variables such as velocity and pressure are shared by the phases and their value is calculated based on an average volume-fraction value in that cell. (ANSYS FLUENT 12.0, 2009)

Figure 3.4 shows representation of air and water phases in simulation H9J of this study. In the figure blue represents the cells filled with air where $\alpha \sim 0$ and red represents the cells filled with water, where $\alpha \sim 1$.

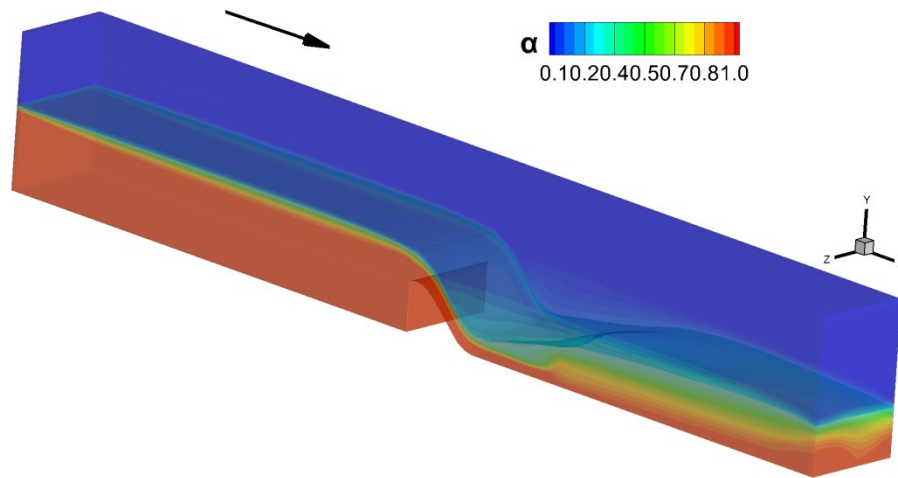


Figure 3.4 Volume Fraction of water for case H9J

3.2.6 Dimensional Analysis

In our study to determine the effects of discharge and roughness, sixteen cases were carried out as shown in the Table 3.2. As aforementioned in “Introduction” section, the scale of the model used is suitable for physical experiments in laboratories. In order to investigate the effect of scale, the previously simulated D6 case is selected. The dimensions used in D6 simulation is assumed as model dimensions. Then, two length scales are arbitrarily selected as $L_R = 1/25$ and $L_R = 1/50$. These length scales are assumed to represent the ratio of model dimensions to prototype dimensions. Therefore, the model dimensions of D6 are multiplied by 25 to obtain the prototype dimensions of case P25, whereas the model dimensions of D6 are multiplied by 50 to obtain prototype dimensions of case P50. The Froude similarity is used to re-scale the prototype cases, where Froude number of the model, Fr_m , is assumed to be identical to the Froude number of the prototype, Fr_p . The calculations of model and prototype dimensions with respect to scale multipliers are given below.

Model D6 :

In D6 case design discharge (Q_d) is $0.027 \text{ m}^3/\text{s}$, roughness height (k_s) is 0.07 mm , water depth (H_{inlet}) is 0.3 m , width of the channel (B_{inlet}) is 0.403 m and area of the inlet (A_{inlet}) is 0.1209 m^2 . Using the area of the inlet and design discharge, the average velocity at the inlet (V_{inlet}) is calculated as $V_{inlet} = Q/A = 0.027/0.1209 = 0.223 \text{ m/s}$. Based on this average velocity and the depth of flow, the Froude number of the model (Fr_m) is calculated as $Fr_m = V/\sqrt{gH_{inlet}} = 0.13$. This value is used in the Froude similarity analyses. The model is assumed to be reduced with length scales (L_R) of $1/25$ and $1/50$. Using Froude similarity and length scales, new discharge Q_p , new existing head conditions H_p are calculated. Using prototype scales, two new simulations are carried out to investigate the scale effects.

Prototype P25 (25/1) :

The length scale is taken as $L_R = L_m/L_p = 1/25$ for the calculations. By Froude similarity, $Fr_p = Fr_m = 0.13$, $B_p = 0.403 \times 25 = 10.075 \text{ m}$, $H_p = 0.3 \times 25 = 7.5 \text{ m}$, and $k_s = 0.07 \times 25 = 1.75 \text{ mm}$. The Froude number of the prototype is expressed as $Fr_p = V_p/\sqrt{gH_p}$, $V_p = 0.13 \times \sqrt{9.81 \times 7.5} = 1.1150 \text{ m/s}$. Therefore, the discharge of the prototype case P25 is calculated as $Q_p = 1.1150 \times A_p = 84.26 \text{ m}^3/\text{s}$, where A_p is the area of the inlet of the prototype P25 simulation calculated as $H_p \times B_p$.

Prototype P50 (50/1) :

The length scale is taken as $L_R = L_m/L_p = 1/50$ for the calculations. By Froude similarity $Fr_p = Fr_m = 0.13$, $B_p = 0.403 \times 50 = 20.15 \text{ m}$, $H_p = 0.3 \times 50 = 15 \text{ m}$, and $k_s = 0.07 \times 50 = 3.5 \text{ mm}$. The Froude number of the prototype is expressed as $Fr_p = V_p/\sqrt{gH_p}$, $V_p = 0.13 \times \sqrt{9.81 \times 15} = 1.58 \text{ m/s}$. Therefore, the discharge of the prototype case P50 is calculated as $Q_p = 1.58 \times A_p = 476.64 \text{ m}^3/\text{s}$, where A_p is the area of the inlet of the prototype P25 simulation calculated as $H_p \times B_p$.

In these calculations, L_R is the length scale, Fr_p and Fr_m are prototype and model Froude numbers respectively, B_p is the prototype width, H_p is the depth of water at the inlet of the prototype, k_s is the roughness height over the prototype spillway, V_p is the mean velocity, and Q_p is the discharge in prototype. Relation between model and prototype scale simulations is given in Figure 3.5.

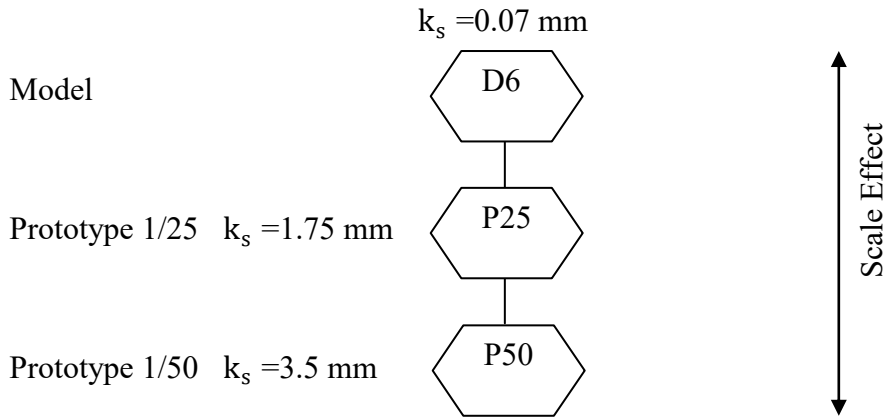


Figure 3.5 Scale effect simulation matrix

3.2.7 Fluent Setup

Pre-processing is done with the GAMBIT which is also a commercial program provided by ANSYS. These studies consist of setting the boundary conditions and creating the geometry and computational grid. After execution of the FLUENT, a Launcher appears on the screen. In this screen some selections should be made. The first (Launcher) screen of the FLUENT is shown in the Figure 3.6. In this screen “3D” flow for the type of flow, “Double Precision” for the solutions and for the processing “Serial Processing” options are selected for this study.

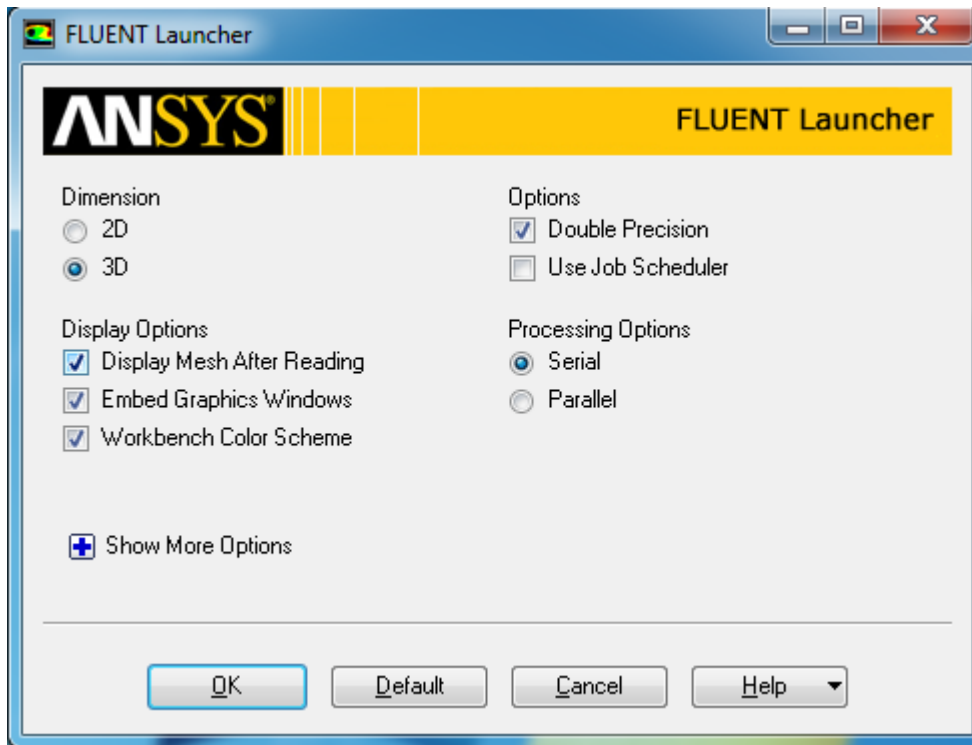


Figure 3.6 FLUENT Launcher Screen

After the first settings by clicking “OK” button the main screen appears which one can import the geometry and make other settings. First, boundary conditions set and geometry created by GAMBIT is imported to the FLUENT. In the “Generals” tab, which is shown in the Figure 3.7, Solver settings and gravity acceleration magnitude, is given and direction is selected. For the type of flow in the calculation “Pressure based” type in order to apply the VOF method and “Transient” flow selected. Velocity formulation is selected as “Absolute”. The flow is set as two-phased flow. The first phase is selected air which program obligates first phase as the fluid has the lower density for a true startup. The second phase is water with density of 998.2 kg/m^3 and dynamic viscosity of 0.001003 Pa.s . For the turbulence closure, SST $k-\omega$ model is selected which is explained in detail in section 3.2.3. All simulations run with fixed time step $\Delta t = 0.001 \text{ sec}$. with maximum 20 iterations per time step. Number of time steps is taken 5000, which means total simulation time is 5 seconds.

In the study of (Dargahi, 2006) it is assumed that the flow would reach steady-state in 5 seconds.

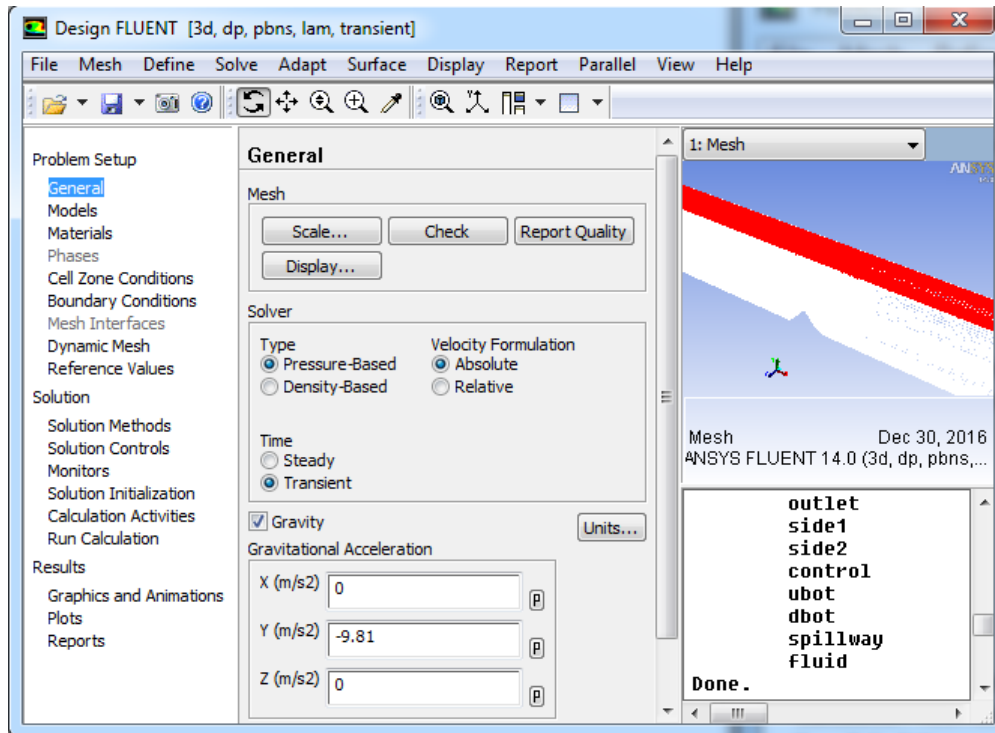


Figure 3.7 General Settings

Run calculation selections are shown in the Figure 3.8. This type of simulation takes approximately 5 days with an Intel P4 Processor and 8 GB Memory desktop PC.

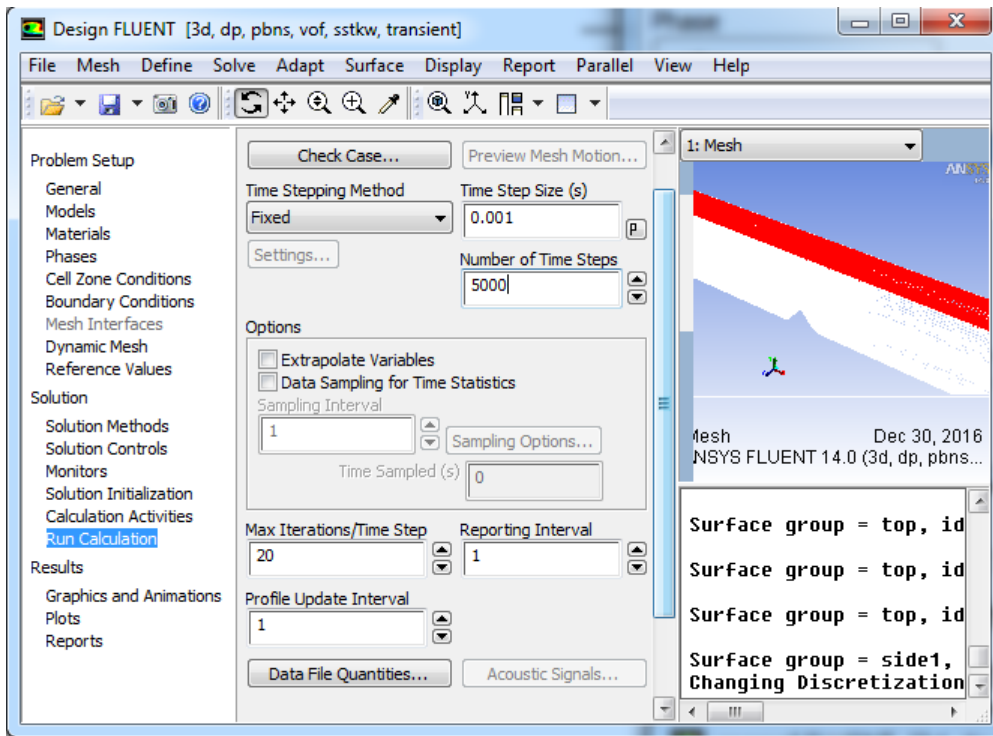


Figure 3.8 Run Calculation setting

CHAPTER 4

RESULTS AND DISCUSSION

4.1 Flow over Spillways under Several Downstream Conditions

In the first part of the discussion, the effect of roughness only as a k_s value in the momentum equation will be considered. The possible effect of material roughness in terms of k_s to flow depth, flow velocity and C_c values used the discharge relations of spillways are investigated. In the second part of the study the downstream depth and formation of simple hydraulic jump at various flow conditions are discussed. Jump lengths obtained through numerical simulations are compared with the well-known empirical relations. Finally, the air entrainment at the jump is evaluated in terms of change of total air concentration in the flow with time.

Figure 4.1 shows the location where h_0 , V_0 , V_c , V_t values are evaluated using simulation data. These values are often referred in the text or in tables in the coming subsections.

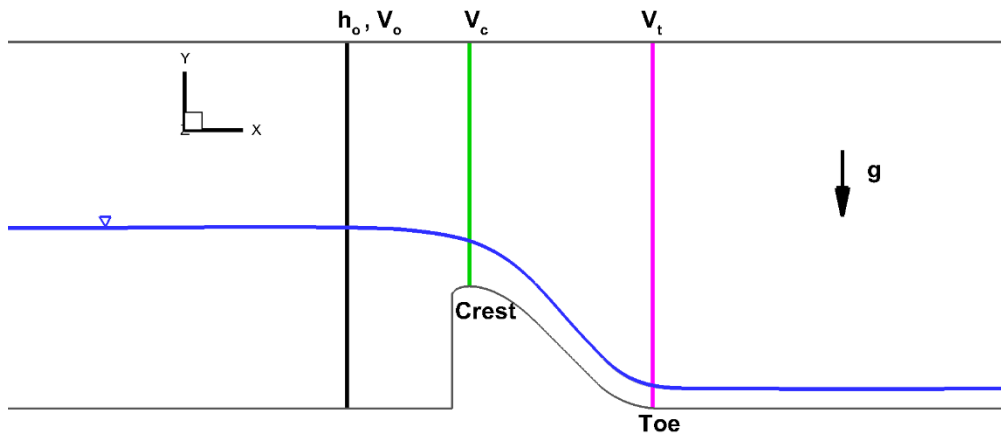


Figure 4.1 Sketch of the domain that shows the location of the numerical measurements upstream over the crest and at the toe of the spillway.

Where, g is gravitational acceleration, h_0 , V_0 , V_c and V_t are spillway operating head, approach velocity, crest and toe velocities, respectively.

Even though the previous studies in literature on much complex flow domain suggests that ANSYS Fluent is a viable tool to simulate flow over spillways, the results from the high flow case with smooth walls was compared to the experimental findings in the study of Dargahi (2006) in Figure 4.2. In this figure the water surface profile in the domain from the current numerical work is compared to the experimental measurements. The numerical and experimental results are in good agreement.

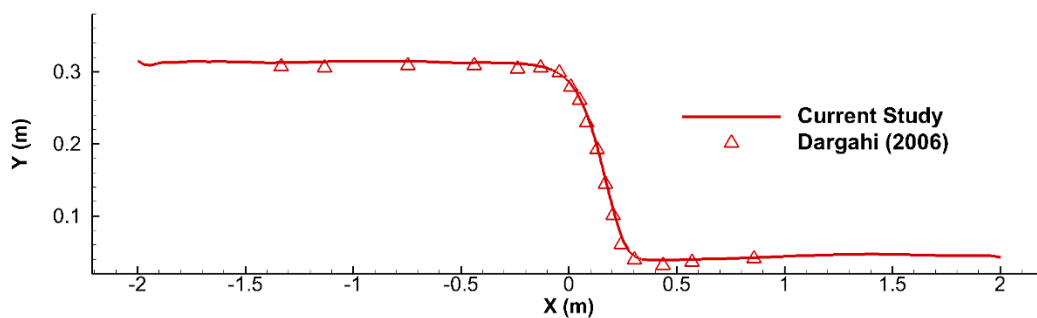


Figure 4.2 Water surface profile for H9 case. Numerical and experimental (Dargahi, 2006) results are compared.

4.1.1 Effect of Roughness on Free Surface

Spillway roughness was accounted by a k_s value in the Navier-Stokes equations. It is not mounted physically on the bounds. As mentioned before, four different roughness heights were used. These are hydraulically smooth ($k_s=0$), smooth sheet steel ($k_s=0.07$ mm), planned wood ($k_s=0.5$ mm), and rough concrete ($k_s=2$ mm). The roughness value k_s is effective only on the curved surface of the spillway, the upstream and downstream channel floors are assumed to be smooth walls together with the sidewalls of the channel. The flow depth does not change significantly among low, design and high flow cases for different k_s values. Very minimal changes on the depth of the flow might be observed slightly upstream and on the downstream side of the spillway. However, these differences are so small that they could be neglected. The free surface of the flow is assumed to pass through $\alpha=0.5$. Figure 4.3 shows the shape and depth of the free surface for three smooth wall cases with low, design and high inflow discharge values.

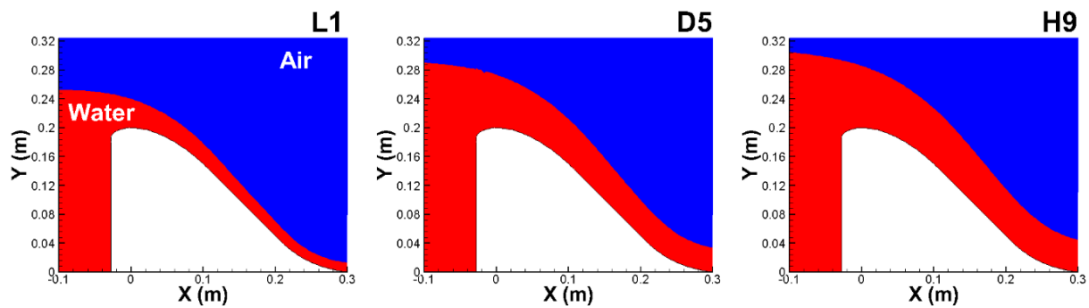


Figure 4.3 Shape of free surface over the spillway. The free surface is assumed to pass through $\alpha=0.5$.

Figure 4.4 shows the small differences on the free surface profiles for low discharge and design discharge cases. The comparison is made between smooth spillway (L1 and D5) and spillway with $k_s=2$ mm (L4 and D8). The free surface profile is shown over the full length of the domain. The difference between L1 and L4, and also

between D5 and D8 are so small that no net conclusion can be deduced in terms of effect of roughness to the flow by simply looking at the free surface profiles.

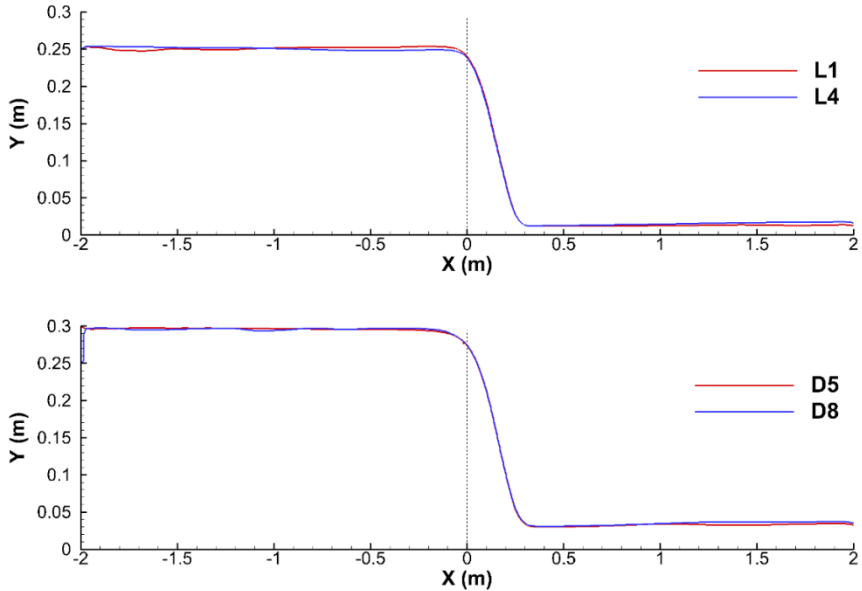


Figure 4.4 Free surface profiles of L1 and L4 (top), and D5 and D8 (bottom).

Further, the near wall velocity of the flow is investigated at a distance 5 cm away from the channel floor over the spillway to assess the effect of roughness to the flow. Figure 4.5 and 4.6 shows the distribution of near wall velocity magnitude over the length of the spillway for L and H cases, respectively. Flow starts decelerating as early as the top of the crest of the spillway in L4 where flow velocity is around 0.5 m/s, while in the smooth wall case L1 in the same region flow velocity is observed to be around 0.7 m/s. In both cases at the toe of the spillway flow reaches velocity values greater than 1.2 m/s. Two solid lines in the figure represent the position of velocity values of 0.9 m/s and 1.2 m/s. In the presence of the roughness, the positions of these contours are observed to be further pushed towards the toe of the spillway.

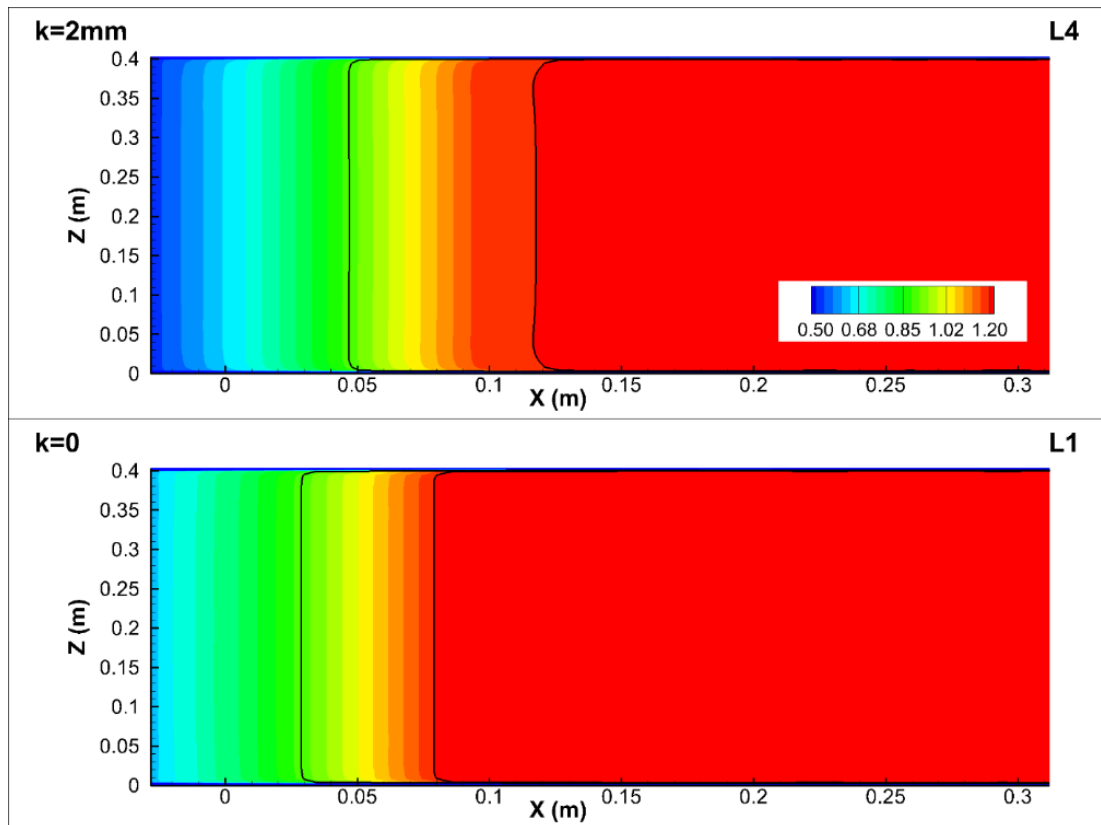


Figure 4.5 Near-wall change in velocity distribution for low flow cases over the spillway.

In higher discharge cases, this retardation of the flow near the spillway surface is much less visible when the surface roughness is only accounted by k_s value in the equations. Only an interesting feature observed in the high flow case is the presence of a somewhat lower velocity patch in between $0.2 < x < 0.27$ m in H12 case compared to the H9 case over a plane 5cm away from the spillway running parallel to the spillway surface.

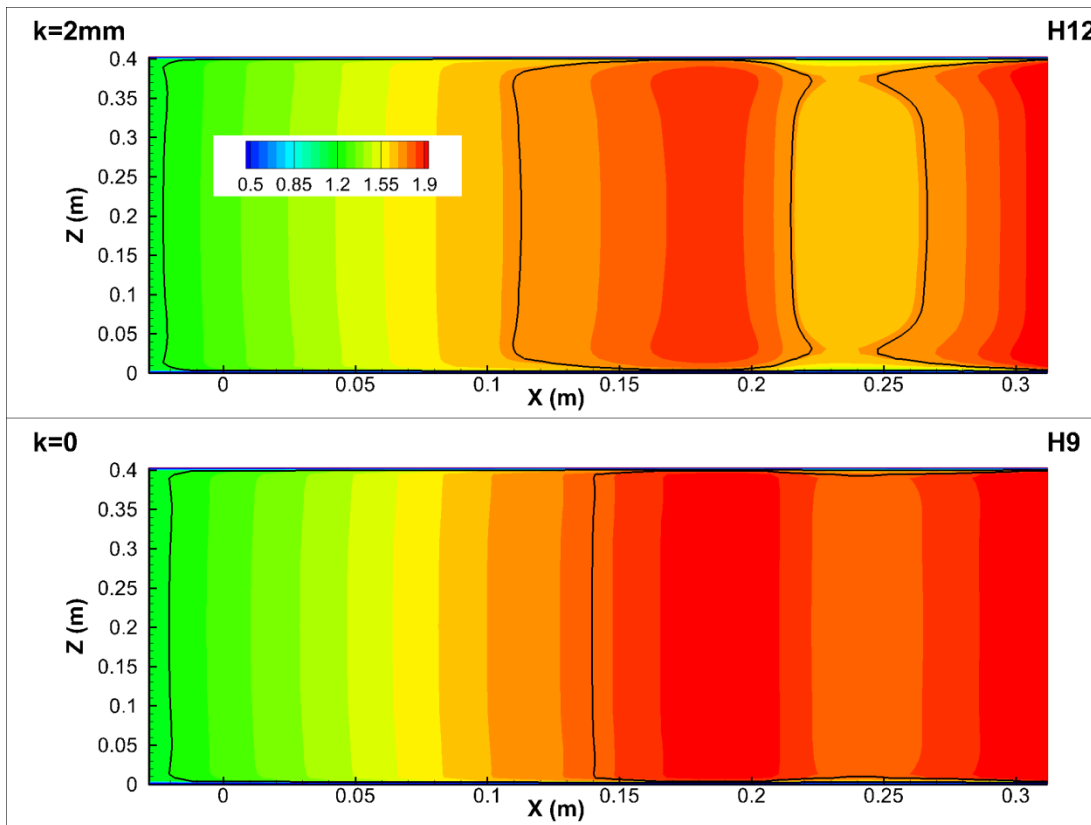


Figure 4.6 Near-wall change in velocity distribution for high flow cases over the spillway.

Figure 4.7 shows the velocity profiles at the toe of the spillway. The velocity profile at the toe of the spillway shows how the flow velocity near the channel bottom decreases with increasing k_s value for low discharge cases. The effect of the roughness value k_s is more pronounced in the low discharge cases due to the lower depth of the flow associated with this discharge. No significant differences are observed for the other two cases in terms of the velocity profile at the toe until the free surface of the flow at $\alpha = 0.5$.

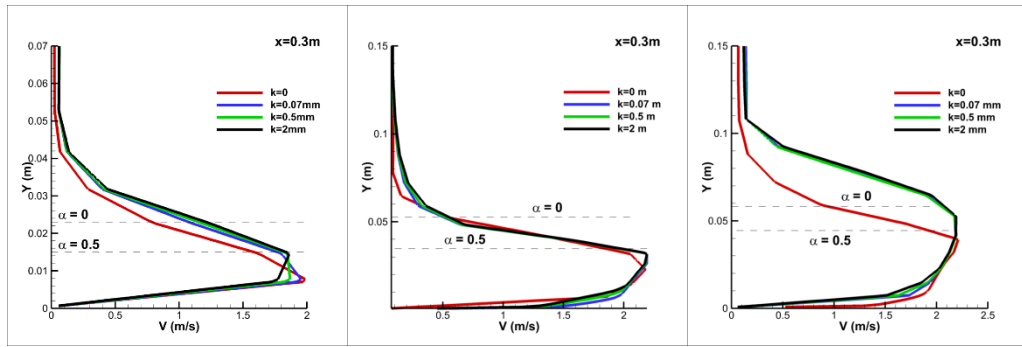


Figure 4.7 Velocity profiles at the toe for L, D and H cases after the rough spillway.

Table 4.1 Comparison of values obtained from CFD, study of Dargahi (2006) and calculation for L cases

Case	h_0 (m)	V_c (m/s)	V_{c-cal} (m/s)	$C_{\eta-cal}$	C_{η} (USACE)	C_{η} k- ϵ RNG (Dargahi, 2006)	C_{η} Exp. (Dargahi, 2006)
L1	0.0477	0.611	0.656	0.73	0.68	0.7	0.68
L2	0.0498	0.658	0.683	0.68	0.68	0.7	0.68
L3	0.0487	0.543	0.587	0.70	0.68	0.7	0.68
L4	0.0483	0.552	0.594	0.71	0.68	0.7	0.68

Table 4.2 Comparison of values obtained from CFD, study of Dargahi (2006) and calculation for D cases

Case	h_0 (m)	V_c (m/s)	V_{c-cal} (m/s)	$C_{\eta-cal}$	C_{η} (USACE)	C_{η} k- ϵ RNG (Dargahi, 2006)	C_{η} Exp. (Dargahi, 2006)
D5	0.0960	0.892	0.960	0.76	0.74	0.756	0.745
D6	0.0941	0.929	0.967	0.79	0.74	0.756	0.745
D7	0.0974	0.922	0.949	0.75	0.74	0.756	0.745
D8	0.0992	0.921	0.950	0.73	0.74	0.756	0.745

Table 4.3 Comparison of values obtained from CFD, study of Dargahi and calculation for H cases

Case	h_0 (m)	V_t (m/s)	V_{t-cal} (m/s)	$C_{\eta-cal}$	C_{η} (USACE)	C_{η} k- ϵ RNG (Dargahi, 2006)	C_{η} Exp. (Dargahi, 2006)
H9	0.1159	1.934	2.040	0.77	0.75	0.762	0.747
H10	0.1138	1.815	1.969	0.79	0.75	0.762	0.747
H11	0.1141	1.793	1.924	0.79	0.75	0.762	0.747
H12	0.1134	1.759	1.879	0.79	0.75	0.762	0.747

V_c is the average velocity which is calculated by a postprocessing program at the slice taken at the top of the crest ($x=0$), V_t is the average velocity which is integrated by the program at the slice taken at the toe ($x=0.3$ m), V_{c-cal} is the average velocity at the top of the crest by averaging velocities taken at $0.2h$ and $0.8h$, V_{t-cal} is the average velocity at the toe by averaging velocities taken at $0.2h$ and $0.8h$ and $C_{\eta-cal}$ is the Discharge coefficient at the crest calculated by the Equation (4.1) using the values obtained from simulation.

$$C_{\eta} = \frac{3Q}{2B\sqrt{2g}(h_0+U_a)^{1.5}} \quad (4.1)$$

In Tables 4.1, 4.2 and 4.3, the C_{η} values obtained via USACE formulation and the values from the study of Dargahi (2006) do not account for roughness, therefore, for all the cases listed they only have a single-value representation. $C_{\eta-cal}$ values are calculated using simulation results, and they include the effect of k_s in them. It is observed that the $C_{\eta-cal}$ values fluctuate between cases of L and D simulations due to presence of roughness. However, these differences among cases are very small. $C_{\eta-cal}$ values are often comparable to the findings of Dargahi (2006) and to the values obtained by USACE. The depth averaged velocity values and two-point average velocity values show differences between 3-8%.

4.1.2 Scaling Effect and Cavitation Index Calculations

The scaling effect is investigated by simulating one laboratory scale and two prototype scale cases given as in Section 3.2.6. The laboratory scale simulation is later scaled back to prototype scale for comparison. In Figures 4.8 and 4.9, laboratory scale case D6 is compared to prototype scale cases P25 and P50, respectively. The velocity magnitude contours show some differences over the spillway and at the approach. Lesser differences are observed at far downstream of the spillway. Depth of the flow is quite comparable between the cases as well. These results suggest that scaled numerical modeling has lesser effect on depth and average velocity distribution of the flow over spillways.

In Figures 4.8 and 4.9, the dimensions of D6 are multiplied by $1/L_R$ for ease of comparison. The velocity values are also multiplied by $\sqrt{1/L_R}$.

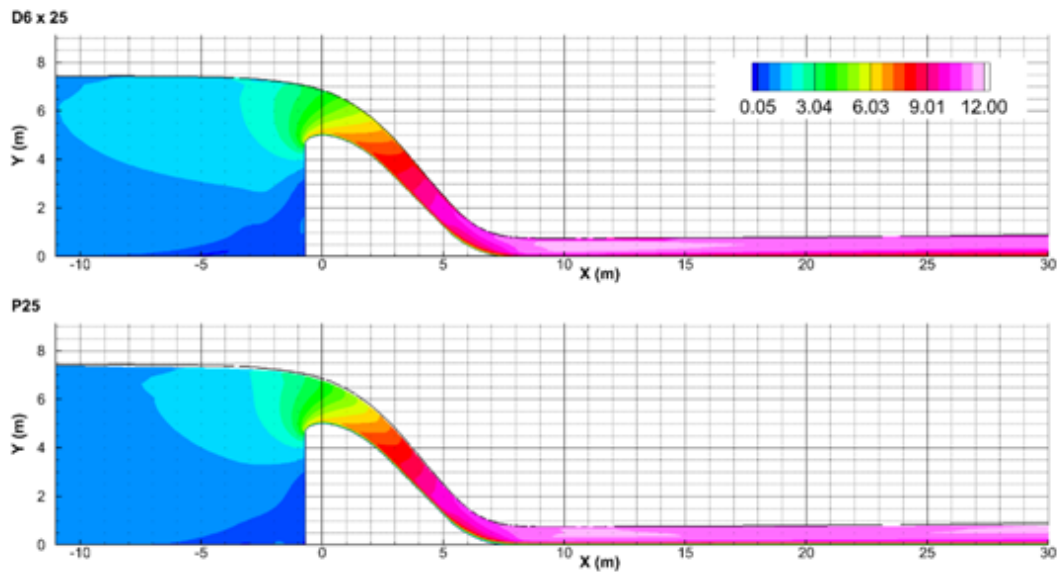


Figure 4.8 Velocity comparisons between D6 x 25 and P25 cases

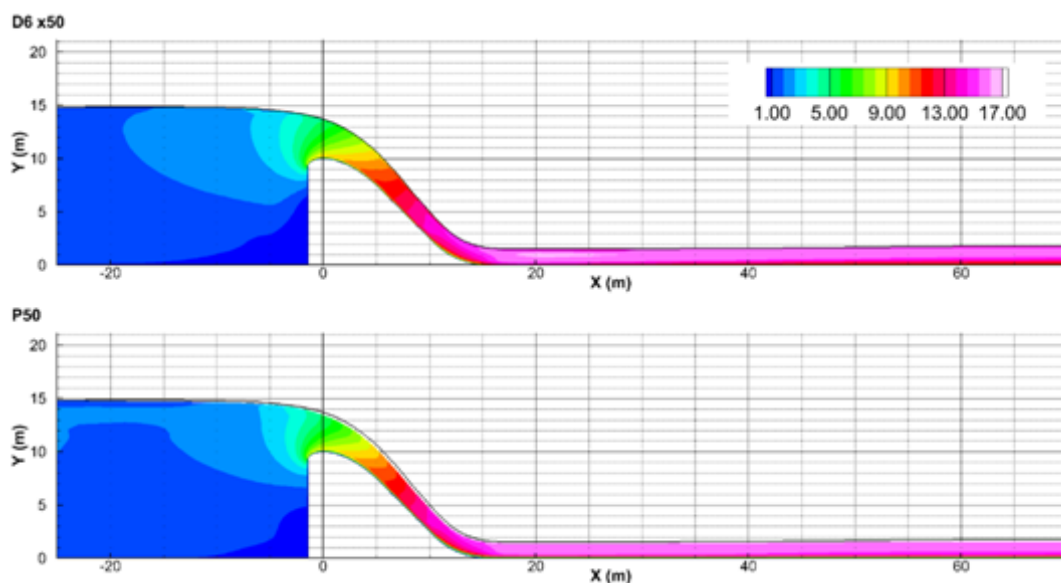


Figure 4.9 Velocity comparisons between D6 x 50 and P50 cases

Cavitation index is calculated using Equation (4.2)(USBR, 2015).

$$\sigma = \frac{P - P_v}{\frac{\rho V^2}{2}} \quad (4.2)$$

The vapor pressure of water at 20°C is used as P_v value in these calculations. P_v is taken as 2.34 kPa (absolute).

Figure 4.10 shows the cavitation index map over the spillway surface. In Equation (4.2), V represents an average flow velocity and often referred in the literature as reference velocity. This velocity value can be taken as the average inflow velocity, which could be calculated as Q/A_i using the discharge and the area of the inlet of each case considered. Based on the dimensional analysis carried out in Section 3.2.6, Table 4.4 is formed. The discharge, inlet area and average inlet velocity of each case considered in Figure 4.10 are listed.

Table 4.4 Discharge, inlet area and average velocity of D6, P25 and P50 cases.

Cases	Length Scale L_R	Inlet Area (m)	Average Inflow Velocity V(m/s)	Q (m³/s)
D6	Model Scale	0.12	0.223	0.027
P25	1/25	75.56	1.115	84.26
P50	1/50	302.25	1.577	476.64

The first row of Figure 4.10 shows the cavitation index, σ , calculated for each case based on average inflow velocity and local pressure values directly taken at a surface running parallel to the spillway about 0.005m from the spillway in D6, 0.125m from the spillway in P25 and 0.25m from the spillway in P50. The distance of the plane parallel to the spillway is selected arbitrarily as 5 mm for the model case of D6. It is scaled for the prototype cases based on the value of length scale, L_R . In the second row of the figure, cavitation index, σ_2 , is calculated based on the local pressure and also the local velocity readings taken directly at the surface of the interest.

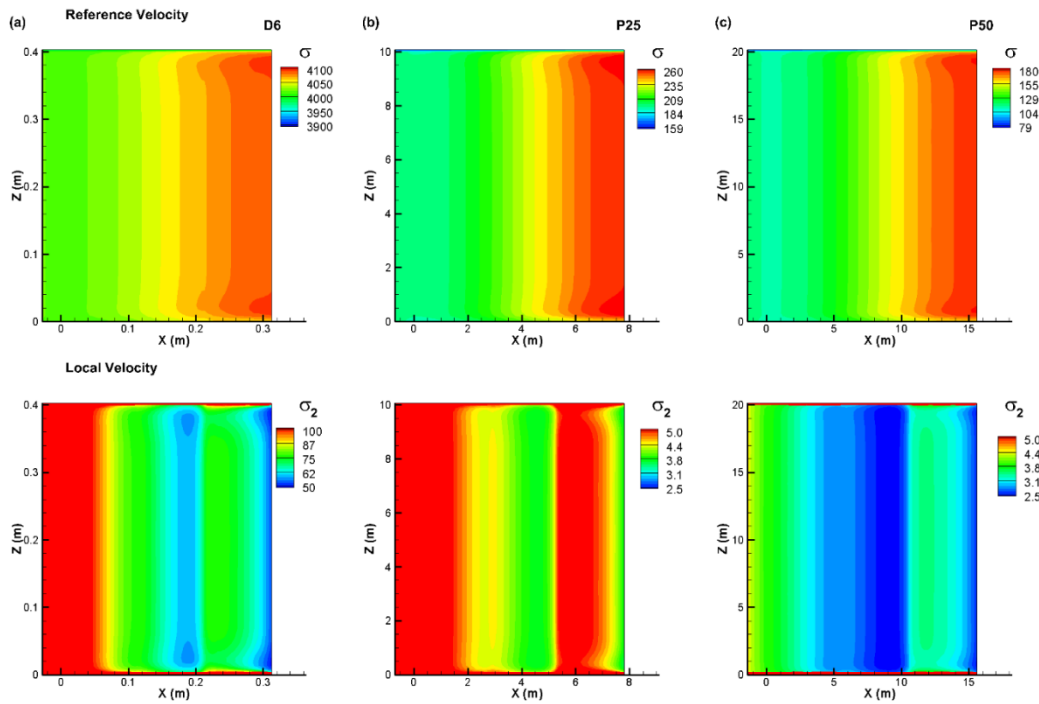


Figure 4.10 Cavitation index comparisons between model (a) and prototype cases (b) and (c)

Even though in none of the cases the cavitation index indicates a possibility of cavitation risk, the values of σ are quite different between prototype and laboratory scales. The trend in the contour plots in the first row are quite similar between cases, indicating lower values of σ near the crest and higher values at the toe. In these frames, a reference velocity is used in the calculation of the index. However, in the second row, the local velocity values are considered in σ calculations and the contour plots are quite different between cases. They are also different from the ones obtained through a constant reference velocity. The range of the σ value changes based on the velocity values used in the calculation. Due to scale effects, the values of both σ and σ_2 are lower in prototype cases compared to model case. Fortunately, the lower values are still in the range where cavitation risk is not expected. However, if the local velocity values are considered in the calculation of σ , the region of relatively lower cavitation indices are calculated to be at the toe and around the

central area of the spillway as shown in the second row of Figure 4.10. These results suggest that numerical simulations should be conducted whenever possible at prototype scale in order to compensate any shortcomings of the laboratory experiments due to scaling. Moreover, local velocity values could be considered together with the reference velocity value to evaluate any possibility of cavitation risk.

Table 4.5 summarizes the basic differences between these cases. In the table the approach depth, h_0 , the depth averaged crest (V_c) and depth averaged toe (V_t) velocities are compared between prototype and laboratory scale cases. Their relative percent errors are given as ϵ . The values listed in Table 4.5 as V_{c-cal} and V_{t-cal} are the average crest and toe velocities calculated based on point velocity readings through simulation results at 20 and 80% of the depth at those locations. Maximum differences are observed for average velocity at the crest and at the toe between D6 and P50 cases.

The approach depth and the velocity of the flow at the crest for D6 is given in Table 4.2. The approach depth h_0 is 0.0941 m and V_c is 0.929 m/s for this case. These values are multiplied by $1/L_R$ and $\sqrt{1/L_R}$ in D6x25 and D6x50, respectively, in Table 4.5.

Table 4.5 Comparison of average velocity values obtained from CFD and at $y=0.2h$ and $y=0.8h$

Case	h_0 (m)	Δh (m)	ε (%)
D6*25	2.3525	0.0828	3.40%
P25	2.4353		
D6*50	4.705	-0.008	-
P50	4.697		
Case	V_c (m/s)	ΔV (m/s)	ε (%)
D6*25	4.645	-0.076	-
P25	4.569		
D6*50	6.569	-0.243	-
P50	6.326		
Case	V_{c-cal} (m/s)	ΔV (m/s)	ε (%)
D6*25	4.835	-0.183	-
P25	4.652		
D6*50	6.838	-0.376	-
P50	6.462		
Case	V_t (m/s)	ΔV (m/s)	ε (%)
D6*25	9.865	-0.353	-
P25	9.512		
D6*50	13.951	-0.28	-
P50	13.671		
Case	V_{t-cal} (m/s)	ΔV (m/s)	ε (%)
D6*25	10.225	-0.287	-
P25	9.938		
D6*50	14.46	-0.507	-
P50	13.953		

4.1.3 Development of Simple Hydraulic Jump at the Apron for Various Discharge and Downstream Boundary Conditions

Conditions that lead to simple hydraulic jump downstream of the spillway are imposed as boundary conditions at the far end of the simulation domain. The formation of the hydraulic jump, its location, its length and the amount of air entrained on the downstream of the spillway after the formation of the jump are discussed in this section.

Figure 4.11 shows simple hydraulic jump formed by imposing a downstream depth for L1 case. The streamlines are used to identify the start and end of the hydraulic jump. The location of start of the jump is selected where streamlines start curving up. The location of end of the jump is selected where streamlines run almost parallel to one another.

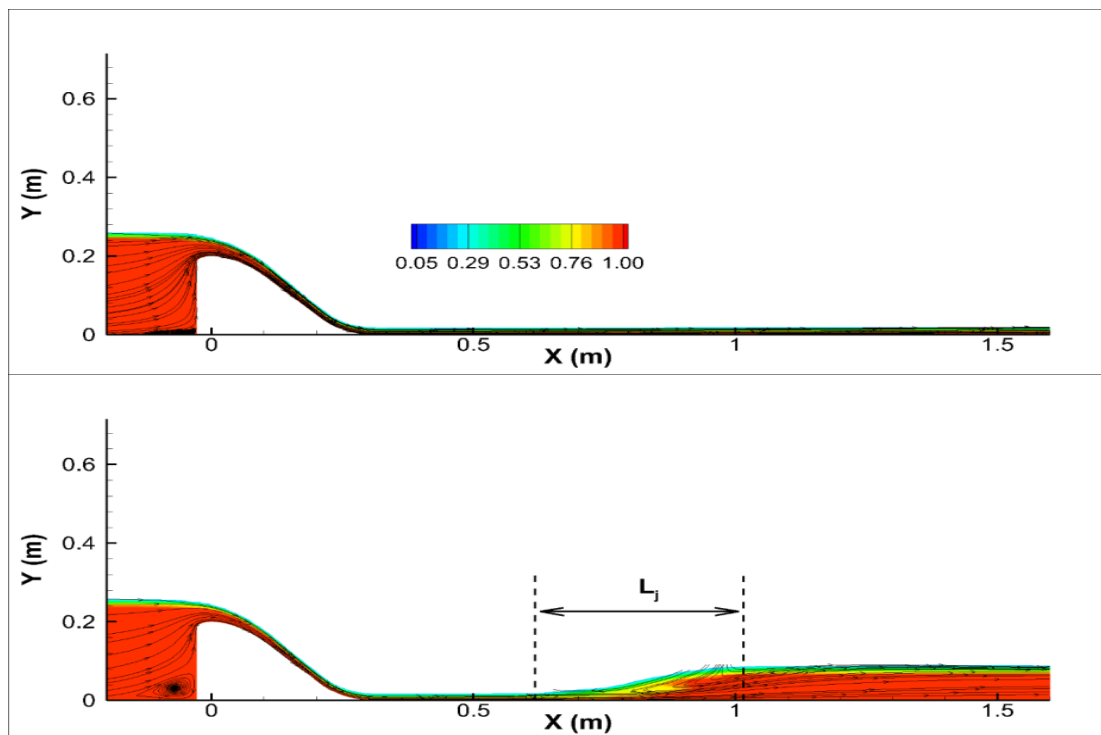


Figure 4.11 Simple hydraulic jump in low discharge case, L1J

Figure 4.12 shows the jump for design discharge, D5. The jump characteristic looks quite different from the jump that form due to low discharge shown in previous figure.

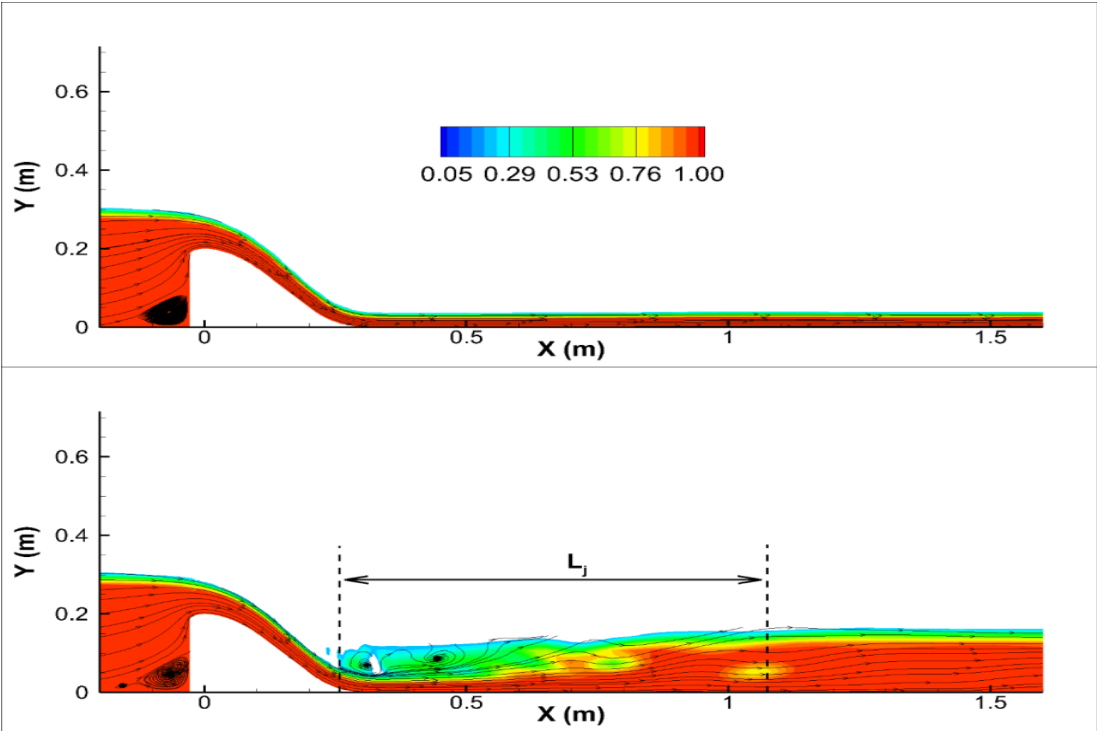


Figure 4.12 Simple hydraulic jump in design discharge case, D5J

During the simulation the formation of the jump with the release of the flow could be observed in time. Figure 4.13 shows the progress of the flow and formation of the jump of D5J. Once the jump forms due to imposed downstream depth condition at the exit section, it travels upstream until it reaches a stable condition, where specific force F_1 on the upstream side and the specific force F_2 on the downstream side equalize. For D5J this takes about 8s in the simulations. Once the jump settles to its location, it does not move as significantly upstream and/or downstream, however in this case for instance free surface oscillations are visible, which in return affects the air entrainment. The free surface oscillations of D5J are given in Figure 4.14.

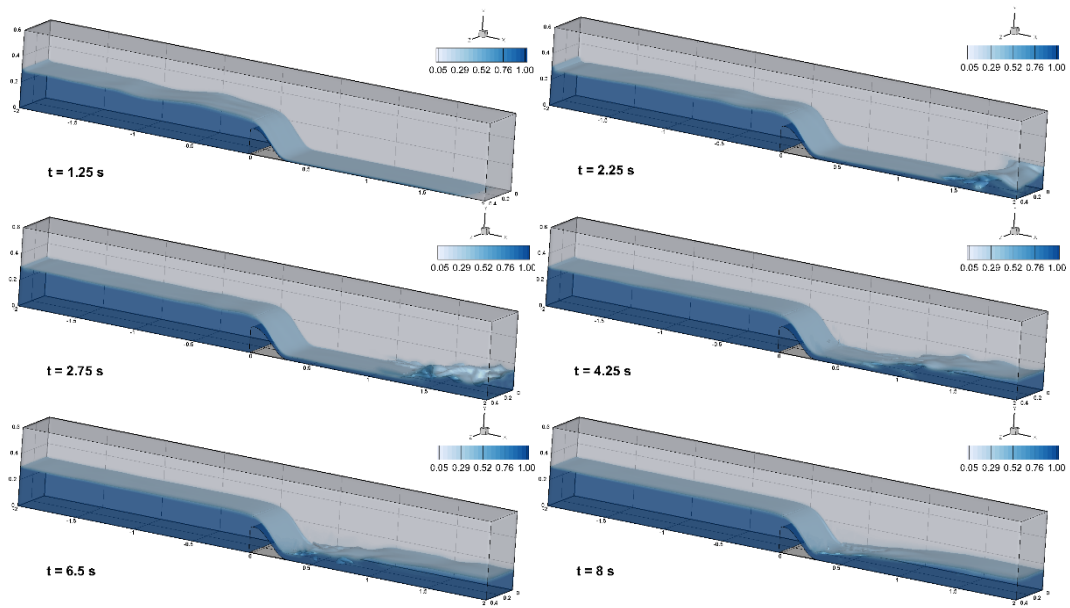


Figure 4.13 Formation of the jump at the downstream of the apron for the design discharge case, D5J, and its evolution towards spillway

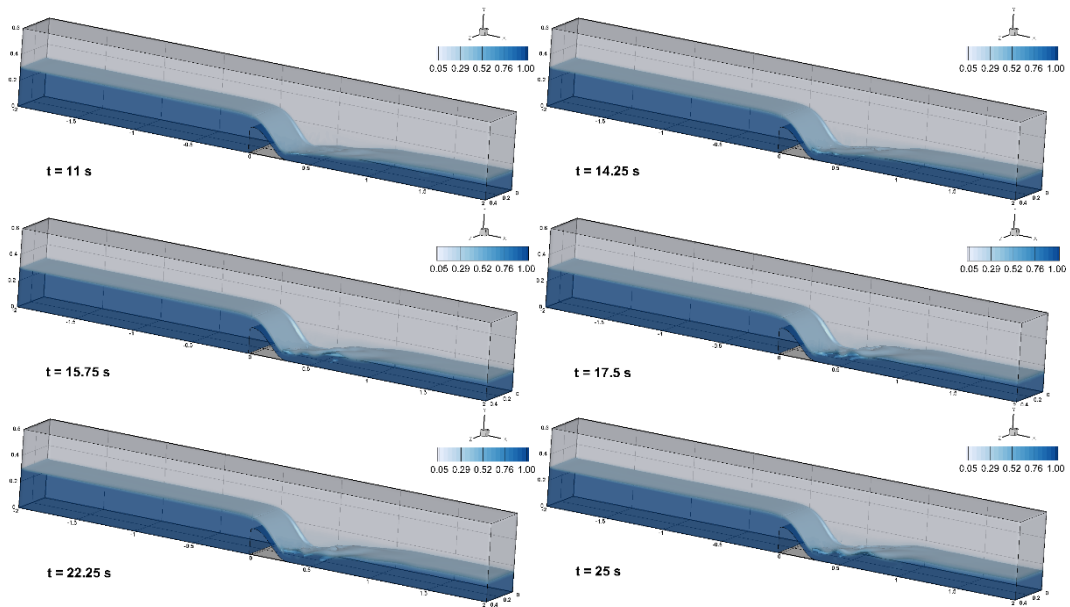


Figure 4.14 Free surface oscillations after jump settles at its position at the toe of the spillway for D5J

Formation of a jump for high flow conditions is visualized in Figure 4.15. The volume fraction representation shows differences between low, design and high discharge cases. For instance in high discharge cases compared to other two more air content inside the jump formation is observed.

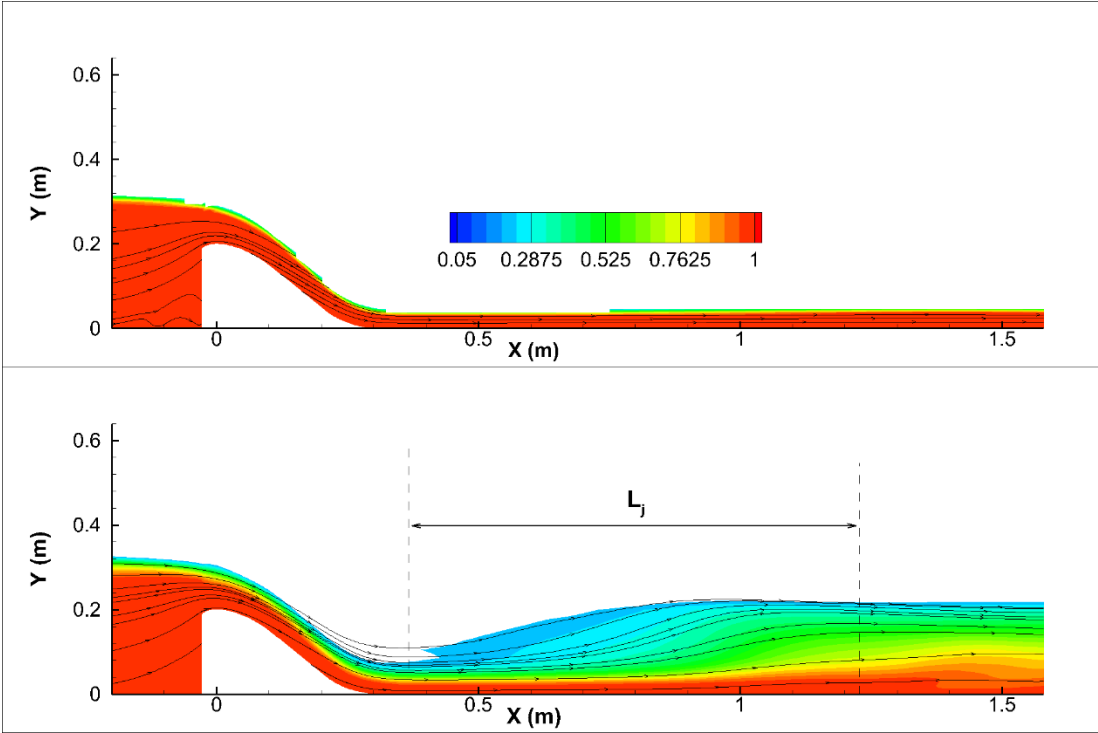


Figure 4.15 Simple hydraulic jump in high discharge case, H9J

A choked jump case is simulated using the inflow conditions of H9, however, the imposed exit conditions allows the formation of a choked jump. The downstream depth at the exit is taken quite comparable to the depth of the flow behind the spillway. This case is listed as H9J2 in Table 3.2. The progress of the flow after the release could be observed over time in Figure 4.16. Formation of the roller and its motion upstream can be observed after $t > 2s$. In about 5s with given conditions, a choked jump forms over the spillway surface.

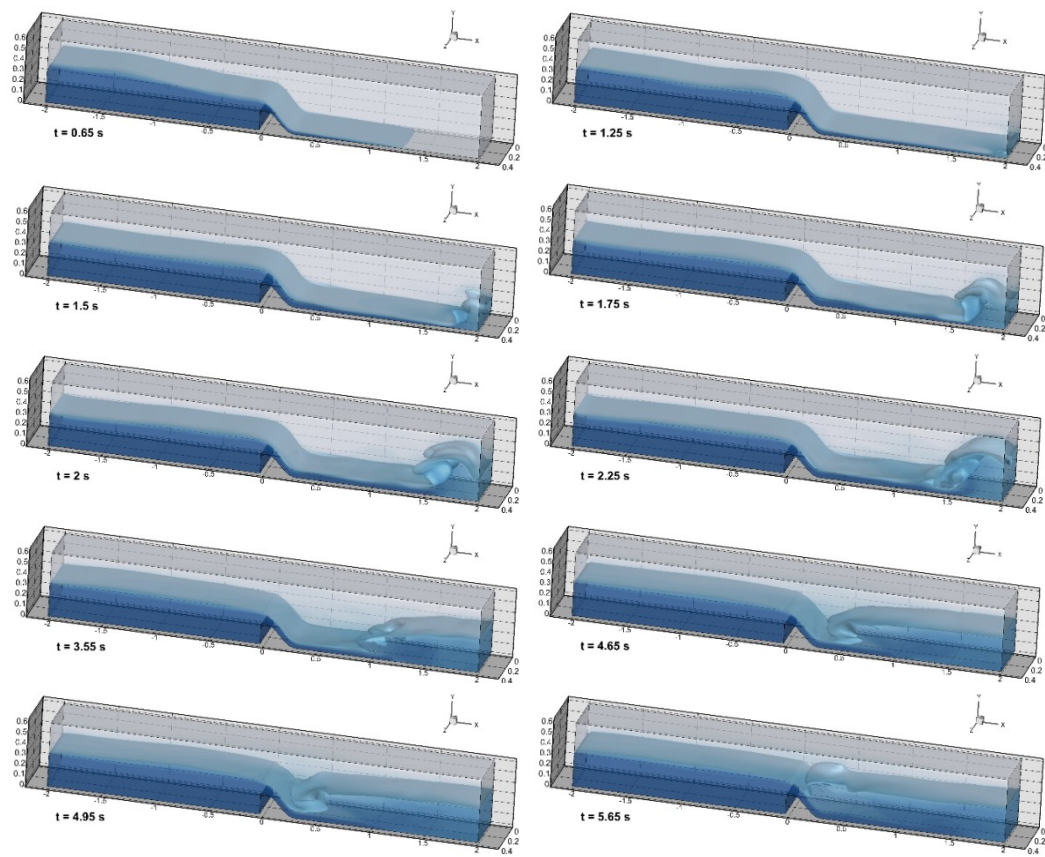


Figure 4.16 The formation and evolution of a choked jump for high discharge case, H9J2

4.1.4 Air Entrainment as a Consequence of Jump

Air entrainment is calculated based on the volume of air-mixed cells on the downstream side. They are normalized by the total volume of the domain downstream after the crest of the spillway. The cells that make up the air-mixed volume is arbitrarily assumed to have $0.25 < \alpha < 0.75$. This region is visualized with these limit iso-contours in figures of this section. The instances given in iso-contour figures are indicated on line plots with red dashed line. In the flow domain α values less than 0.25 are neglected and assumed as air-only regions.

The change in air content of the L1J jump is given in Figure 4.17. The air content increases abruptly with the formation of the jump. The volume of the aerated flow shows oscillations. These oscillations are relatively larger till the jump settles at its location. After it settles at around $t=3s$, the oscillations are smaller and an average volume of aerated flow in the limited volume of the simulation domain could be calculated at around $0.0001V_o$.

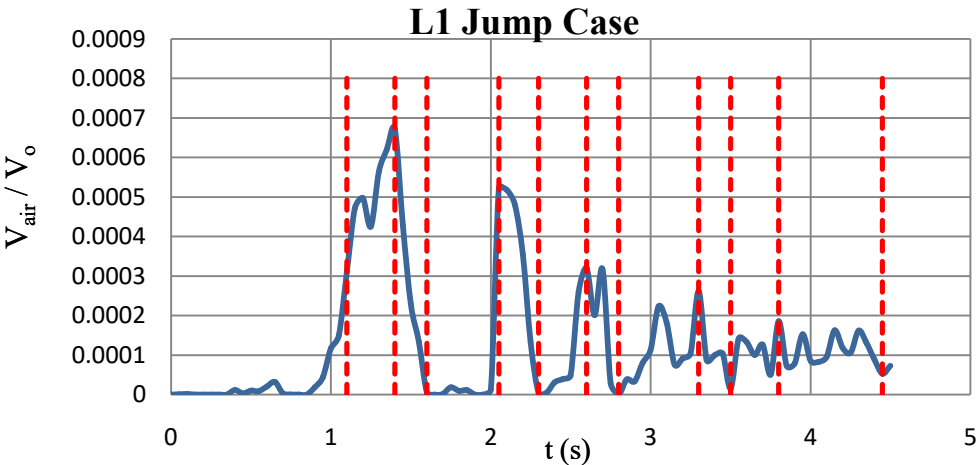


Figure 4.17 Air entrainment evolution with respect to time for L1J Case

In the case of D5J and H9J, the volume of the aerated flow increases in time after the formation of the jump. Even after the jump settles at its final location, the air entrainment keeps increasing. The evolution of the flow and changes in aerated volume for L1J case is given in Figures 4.17, 4.18 and 4.19 and for D5J case in Figures 4.20 and 4.21. Both of these cases could be classified as oscillating jumps. These jumps are observed to have rigorous undulations at the free surface at the free surface. These undulations increase the air content downstream of the spillway structure after the jump. The evolution of the flow and change in aerated volume for H9J case are visualized in Figures 4.22, 4.23 and 4.24.

In Q1 simulations, the jump characteristic in terms of upstream Froude number is similar to L1J case. Both these cases could be considered as steady jumps. Similarly, Q1 case shows that the air-entrainment converges to an average value after the location of the jump and undulations over the free surface settle. Q1 plots are presented in Figures 4.25, 4.26 and 4.27. The average aerated volume towards the end of the simulation time is about $0.006V_0$.

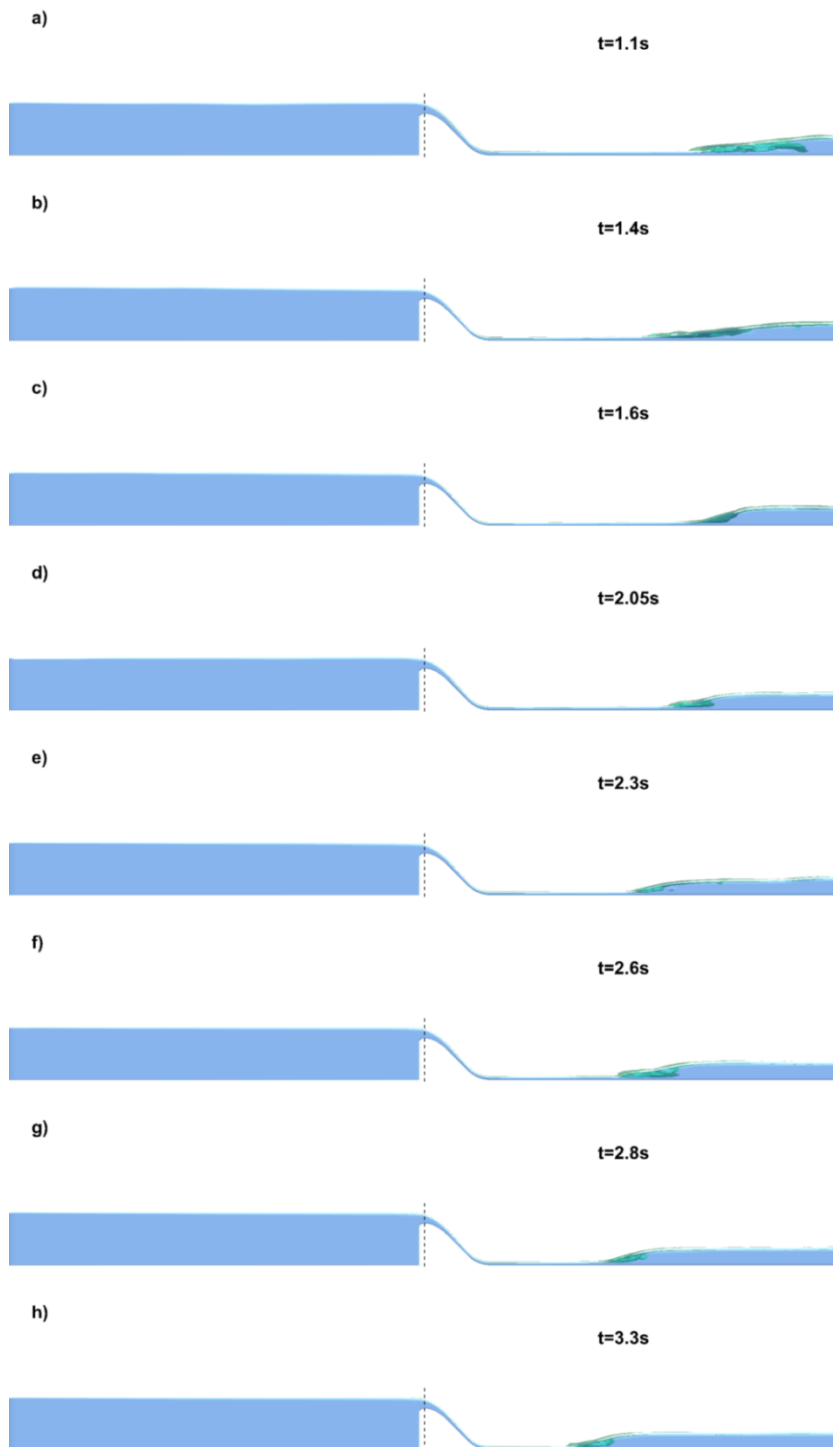


Figure 4.18 Air entrainment evolution at several time instants for L1J Case (a-h).

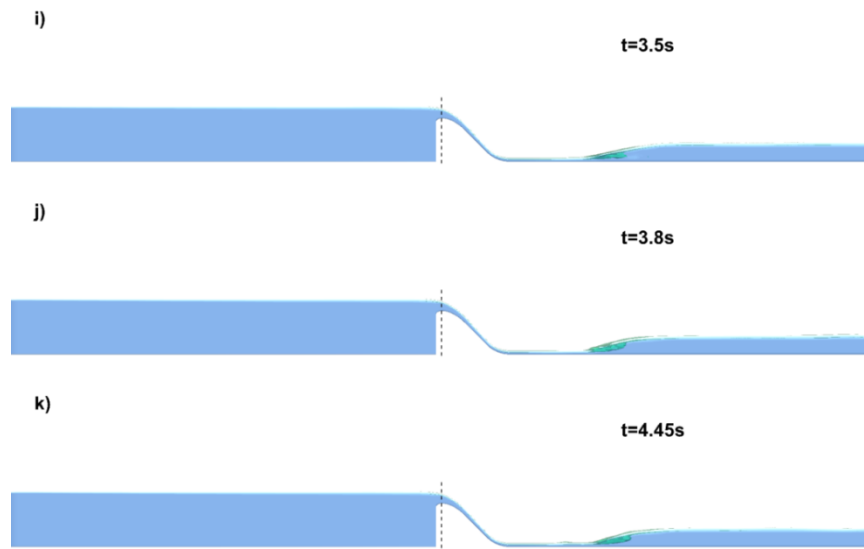


Figure 4.19 Air entrainment evolution at several time instants for L1J Case (i-k)

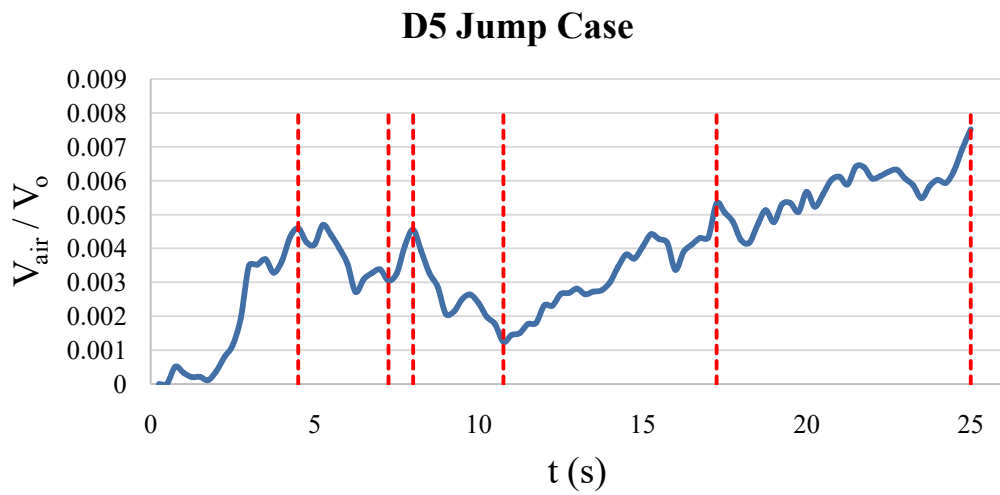


Figure 4.20 Air entrainment evolution with respect to time for D5J Case

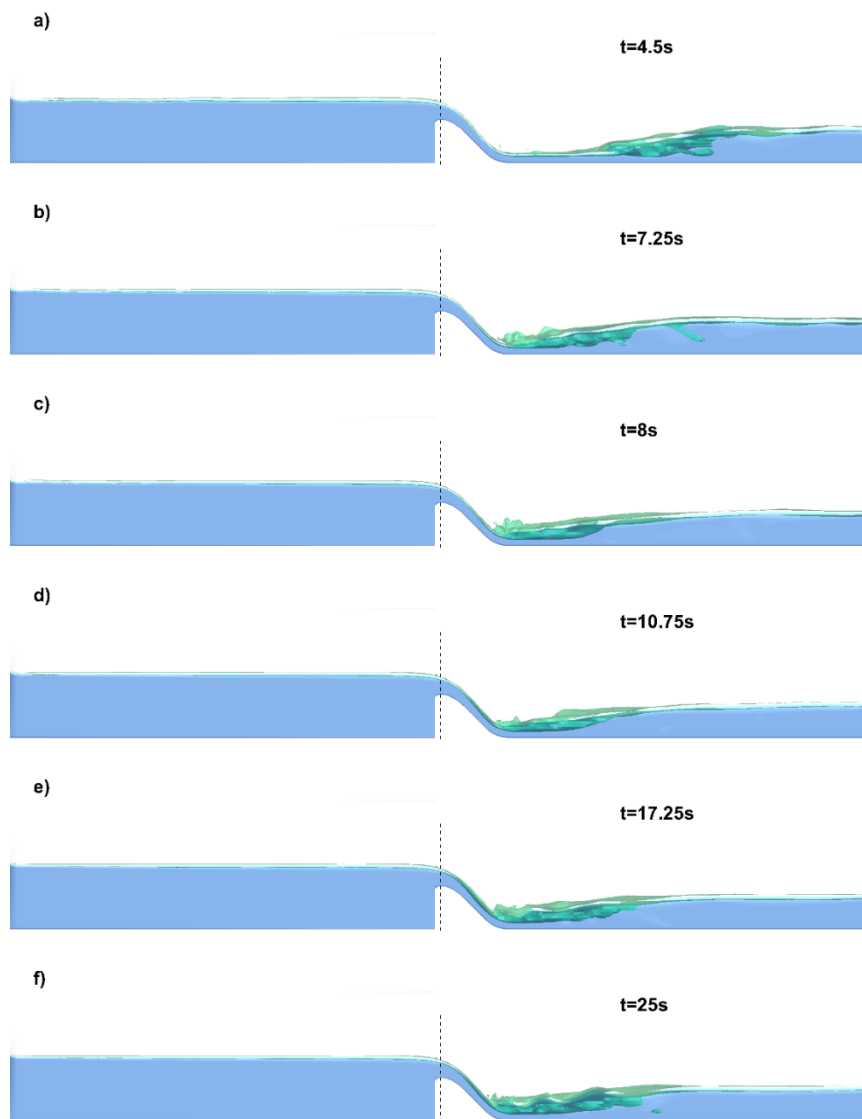


Figure 4.21 Air entrainment evolution at several time instants for D5J Case

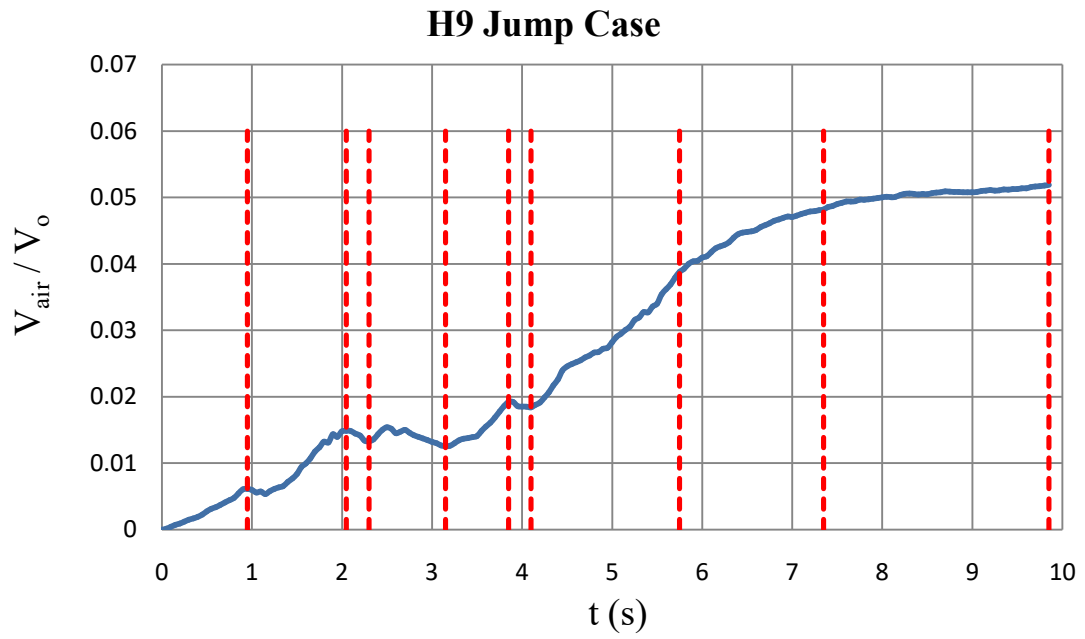


Figure 4.22 Air entrainment evolution with respect to time for H9J Case

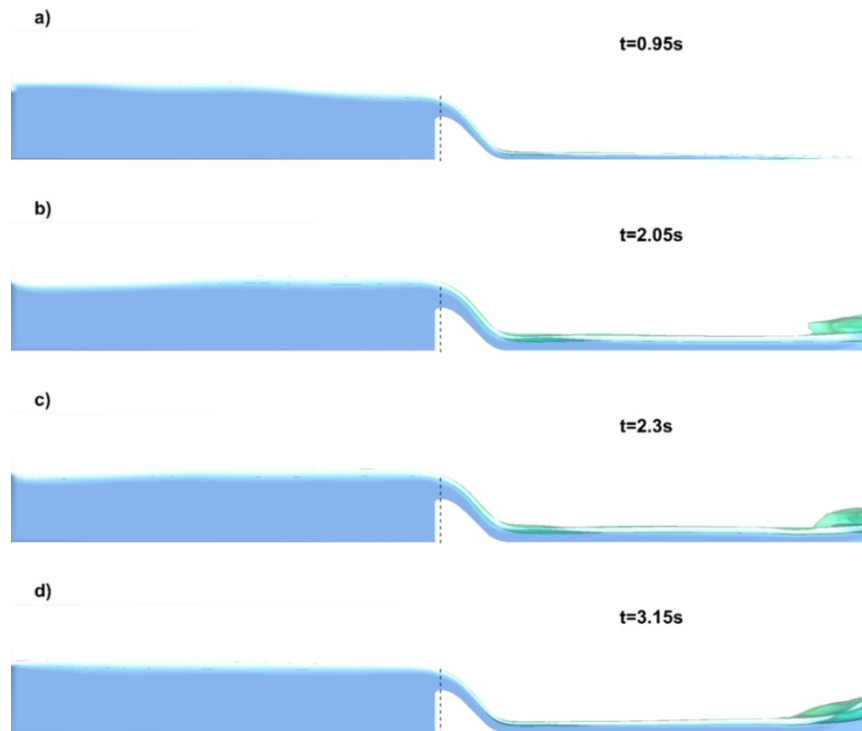


Figure 4.23 Air entrainment evolution at several time instants for H9J Case (a-d)

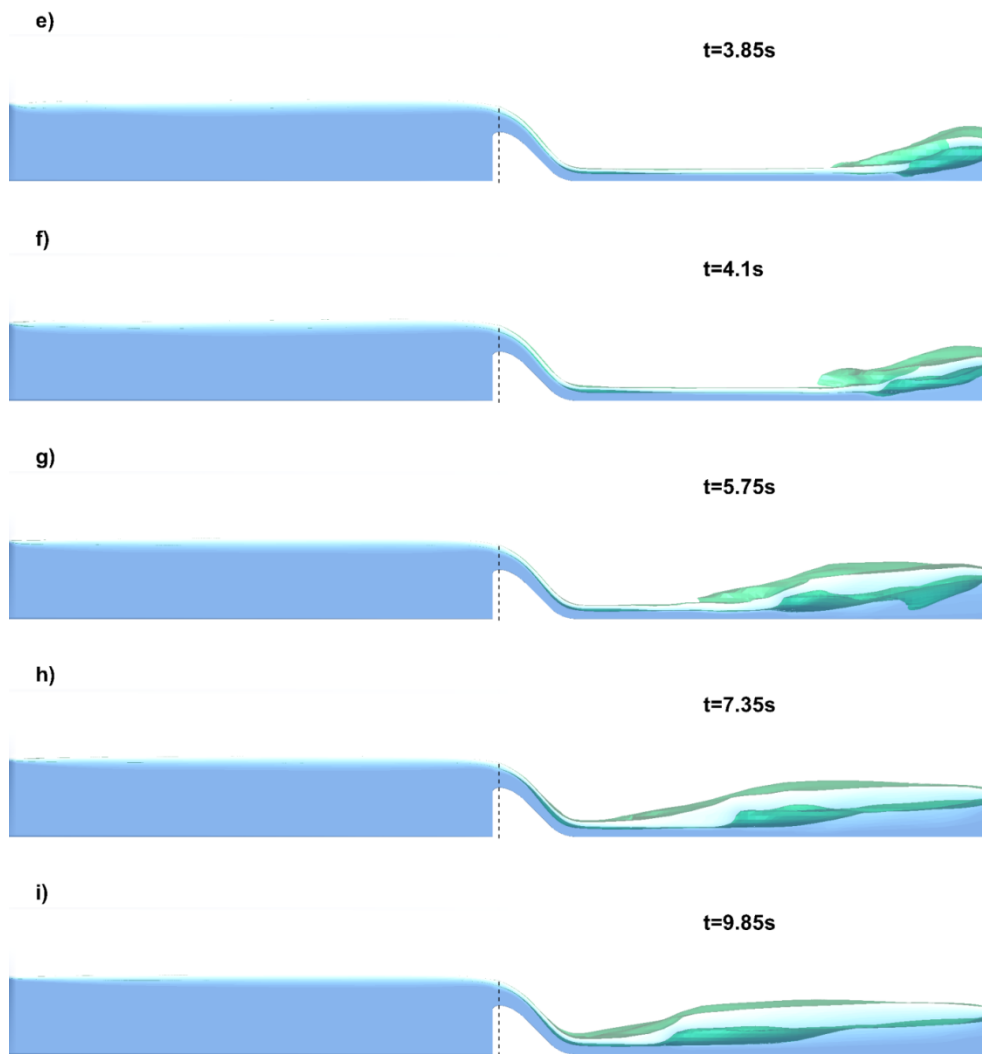


Figure 4.24 Air entrainment evolution at several time instants for H9J Case (e-i)

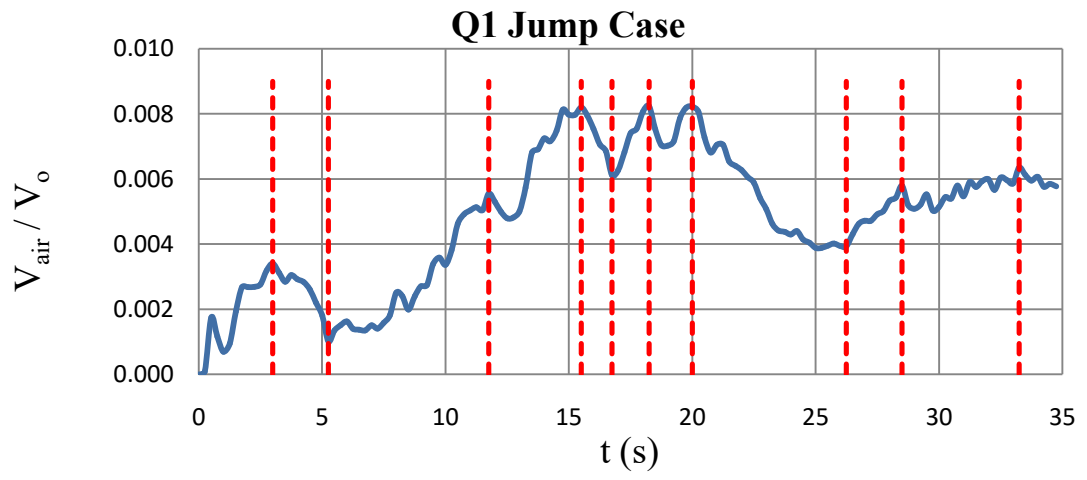


Figure 4.25 Air entrainment evolution with respect to time for Q1 Case

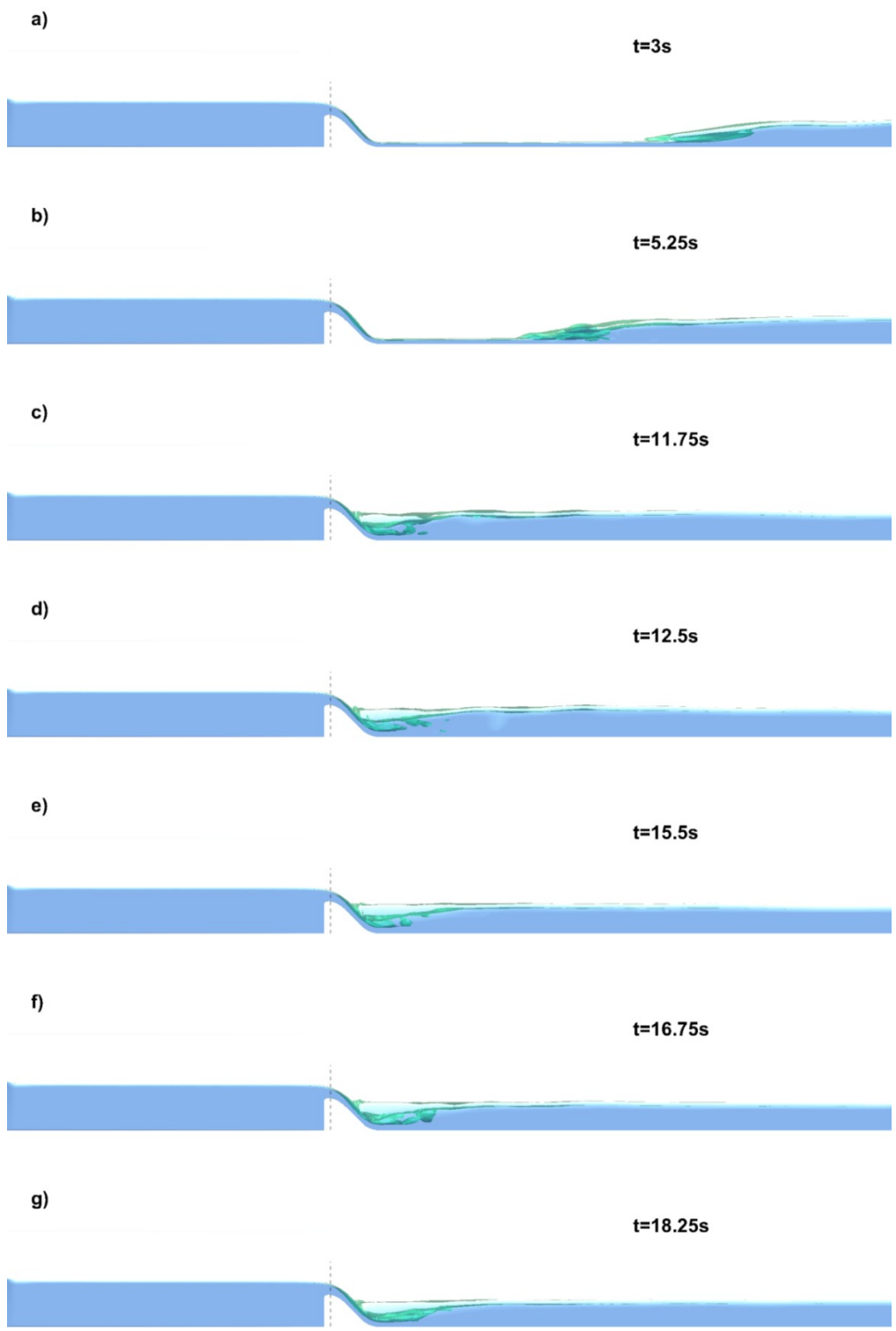


Figure 4.26 Air entrainment evolution at several time instants for Q1 Case (a-g)

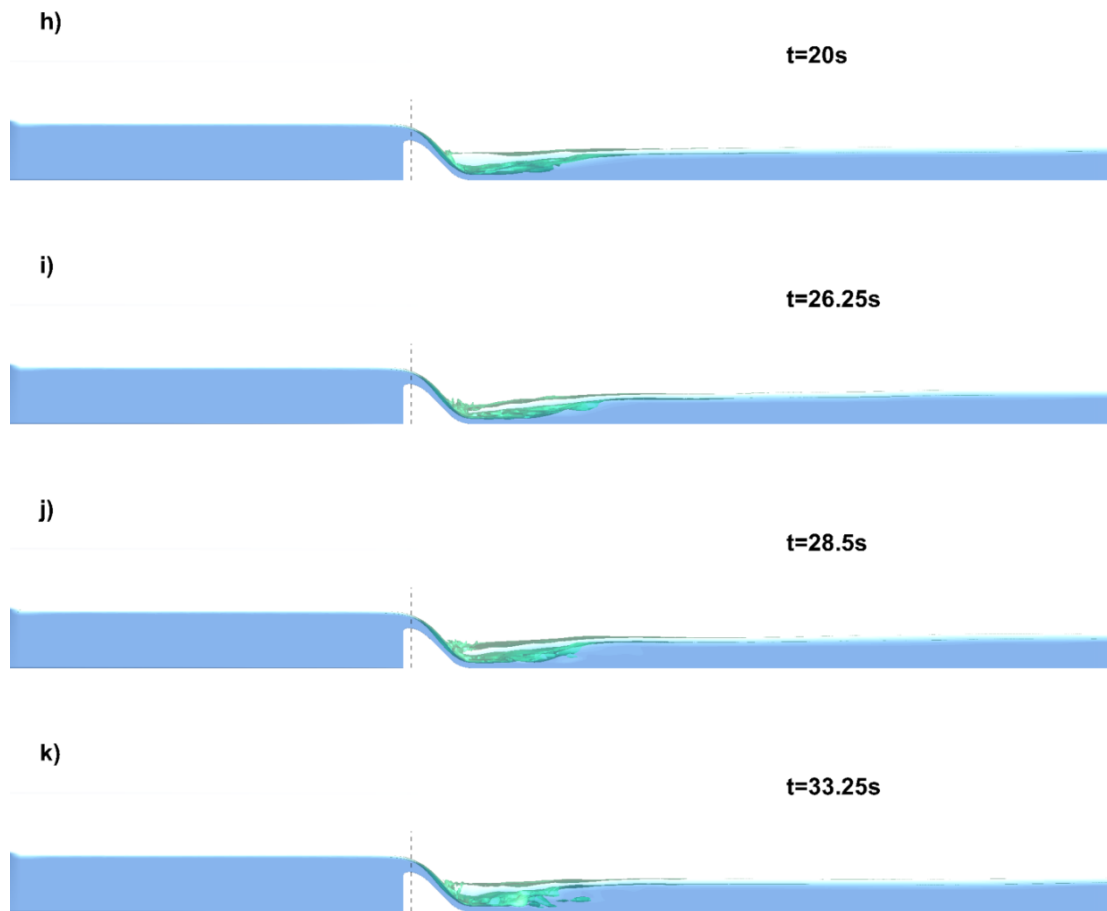


Figure 4.27 Air entrainment evolution at several time instants for Q1 Case (h-g)

4.1.4 Jump Types and Lengths

In order to assess and compare jump lengths, studies of Bakhmeteff and Matzke (1936) and USBR (1955) which are given in Figures 4.28 and 4.29 are used. In addition to these studies, Equation (4.1) and (4.2), which are taken from USACE (1992), are used.

$$L_j = 8y_1 Fr_1 \text{ for } Fr_1 > 5 \quad (4.1)$$

$$L_j = 3.5y_1 Fr_1^{1.5} \text{ for } 2 < Fr_1 < 5 \quad (4.2)$$

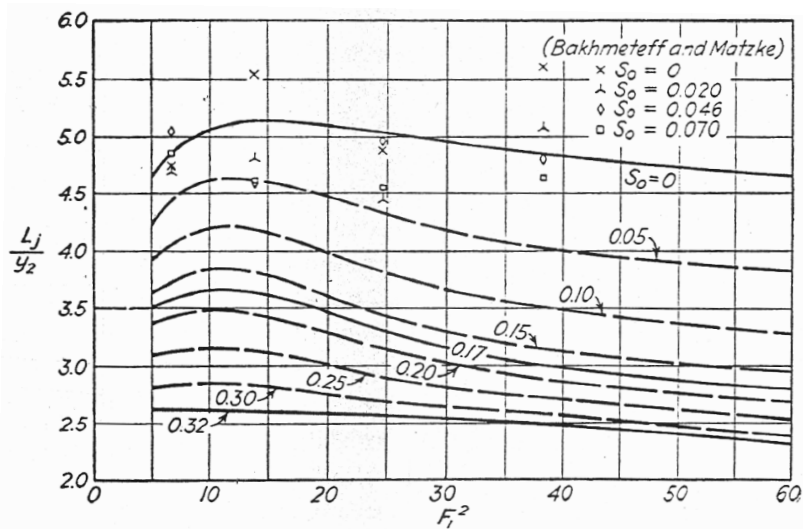


Figure 4.28 Length of jump in sloping channels as a function of F_1 and S_0 (Bakhmeteff and Matzke, 1936)

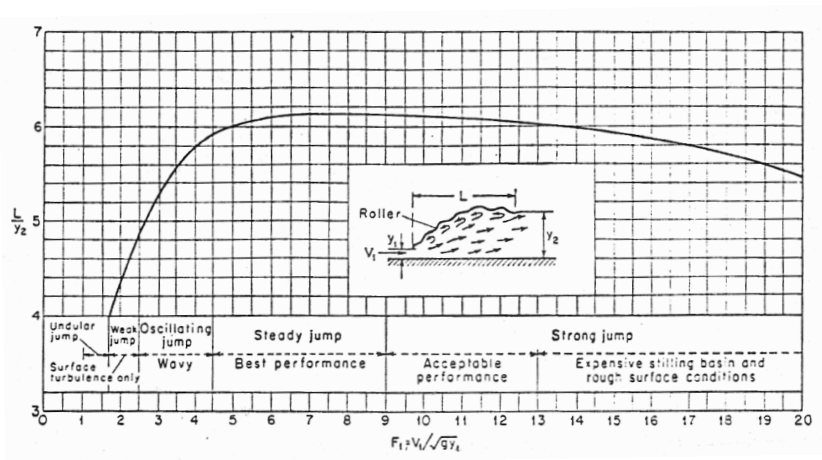


Figure 4.29 Length in terms of sequent depth y_2 of jumps in horizontal channels (USBR, 1955)

Table 4.6 summarizes the downstream depth, discharge, width of the channel, downstream velocity, downstream Froude number, upstream depth, upstream

velocity and upstream Froude number of each jump case. It also classifies the jump based on USBR (1955) classification.

Table 4.7 shows the jump lengths calculated based on simulation results and other studies.

Table 4.6 Values and jump types of jump cases

Case	y_2 (m)	Q (m^3/s)	B (m)	V_2 (m/s)	Fr_2	y_1 (m)	V_1 (m/s)	Fr_1	Remarks
L1J	0.0828	0.009	0.403	0.27	0.30	0.01284	1.74	4.90	steady jump
D5J	0.165	0.027	0.403	0.41	0.32	0.02864	2.34	4.41	oscillating jump
H9J	0.1728	0.036	0.403	0.52	0.40	0.04352	2.05	3.14	oscillating jump
Q1	0.302	0.12	0.806	0.49	0.29	0.04333	3.44	5.27	steady jump
Q2	0.225	0.1	0.806	0.55	0.37	0.05061	2.45	3.48	oscillating jump
Q3	0.21	0.08	0.806	0.47	0.33	0.03849	2.58	4.20	oscillating jump

Table 4.7 Comparison of jump lengths obtained by CFD, Bakhmeteff and Matzke (1936), USBR (1955) and USACE (1992)

		CFD	Bakhmeteff and Matzke (1936)	USBR (1955)	USACE (1992)
Case	Fr_1^2	L_j/y_2	L_j/y_2	L_j/y_2	L_j/y_2
L1J	24.0	5.67	5.1	6.0	5.63
D5J	19.5	5.53	5.1	5.9	6.05
H9J	9.9	4.86	4.8	5.4	5.11
Q1	27.8	6.25	5.0	6.04	5.52
Q2	12.1	6.69	5.1	5.6	5.89
Q3	17.6	6.97	5.1	5.9	4.91

The jump length calculated using CFD and other methods are in good agreement. The results are better matched for steady jumps between CFD and USACE (1992).

Even for simulated cases, it is found to be quite difficult to measure the jump length as the free surface oscillations and changes in streamlines in that region makes it hard to determine the exact position of end of the jump. The highest difference is between CFD results and results based on Bakhmeteff and Matzke (1936). The average difference between these results is about 11%. While the average difference between CFD and USBR (1955) is about 4%, whereas this difference is about 6% for CFD and USACE (1992). As mentioned for L1J and Q1 cases, difference between CFD and USACE (1992) is as small as 0.7% and 2.6%, respectively.

CHAPTER 5

CONCLUSION AND FUTURE WORK

5.1 Conclusion

Current study shows that if the roughness is accounted only as a constant in governing equations in RANS simulations its effect may not be captured pronouncedly. There may be more realizable if it is mounted physically on the model.

It would be more appropriate to conduct the numerical study on prototype scale especially if investigating for cavitation.

Hydraulic Jump measurements are much easier numerically especially in terms of jump length and free surface conditions. However determining the length of oscillating jump is still problematic due to free surface oscillations.

It is observed that after jump settles down in its final location, if the jump can be classified as steady jump, air entrainment reaches an almost constant value over time.

In the oscillating jump it is observed that air entrainment is more complex and aerated flow volume increases continuously throughout the simulation time.

5.2 Future Work

Roughness may be accounted physically on the model and its influence may be more realizable.

A study with wider range of Fr numbers could be conducted in order to assess air entrainment through jumps more accurately.

In oscillating jump observations, simulation time may be extended to a sufficient value to investigate air entrainment trends more precisely.

For scale effect observations, results may be compared with physical experiments

REFERENCES

- Akoz, M. S., Kirkgoz, M. S. and Oner, A. A. (2009) 'Experimental and numerical modeling of a sluice gate flow', *Journal of Hydraulic Research*, 47(2), pp. 167–176. doi: 10.3826/jhr.2009.3349.
- Ansys (2009) 'Ansys fluent 12.0', *Inc Northbrook IL*, (April), pp. 49–53. Available at:
http://scholar.google.com/scholar?hl=en&q=Ansys+fluent+12.0+theory+Guide&btnG=Search&as_sdt=0,5&as_ylo=&as_vis=0#1.
- Aydin, M. C. and Ozturk, M. (2009) 'Verification and validation of a computational fluid dynamics (CFD) model for air entrainment at spillway aerators', *Canadian Journal of Civil Engineering*, 36(5), pp. 826–836. doi: 10.1139/L09-017.
- Bakhmeteff, B. A. and Matzke, A. E. (1936) 'The hydraulic jump in terms of dynamic similarity', in *Proceedings of the American Society of Civil Engineers*. ASCE, pp. 145–162.
- Bouhadji, L. (2004) 'Three dimensional numerical simulation of turbulent flow over spillways', *ASL-AQFlow Inc*. Available at: <http://aqflow.com/reports/CFDspill2004-LB.pdf>.
- Chanel, P. G. and Doering, J. C. (2007) 'An evaluation of computational fluid dynamics for spillway modelling', *16th Australasian Fluid Mechanics Conference*, (December), pp. 1201–1206.
- Chanel, P. G. and Doering, J. C. (2008) 'Assessment of spillway modeling using computational fluid dynamics', *Canadian Journal of Civil Engineering*, 35(12), pp. 1481–1485. doi: 10.1139/L08-094.
- Chow, V. T. (1959) *Open Channel Hydraulics*, *McGraw-Hill Book Company*. doi: ISBN 07-010776-9.
- Dargahi, B. (2004) 'Three-dimensional flow modelling and sediment, transport in the River Klarälven', *Earth Surface Processes and Landforms*, 29(7), pp. 821–852. doi: 10.1002/esp.1071.
- Dargahi, B. (2006) 'Experimental Study and 3D Numerical Simulations for a Free-Overflow Spillway', *Hydraulic Engng.* 132, 132(September), pp. 899–907. doi: 10.1061/(ASCE)0733-9429(2006)132:9(899).

Fadaei-Kermani, E. and Barani, G. A. (2014) 'Numerical simulation of flow over spillway based on the CFD method', *Scientia Iranica A*, 21, pp. 91–97.

Gessler, D. (2005) 'CFD Modeling of Spillway Performance', in *Proc. of World Water and Env.Resources Congress*. Anchorage, Alaska. doi: [http://dx.doi.org/10.1061/40792\(173\)398](http://dx.doi.org/10.1061/40792(173)398).

Herrera-Granados, O. and KostECKI, S. W. (2016) 'Numerical and physical modeling of water flow over the ogee weir of the new Niedów barrage', *Journal of Hydrology and Hydromechanics*, 64(1), pp. 67–74. doi: 10.1515/johh-2016-0013.

Hirt, C. W. and Nichols, B. D. (1981) 'Volume of fluid (VOF) method for the dynamics of free boundaries', *Journal of Computational Physics*, 39(1), pp. 201–225. doi: 10.1016/0021-9991(81)90145-5.

Ho, D. K. H., Boyes, K. M. and Donohoo, S. M. (2001) 'Investigation of Spillway Behaviour under Increased Maximum Flood by Computational Fluid Dynamics Technique', *14th Australasian Fluid Mechanics Conference*, (December), pp. 577–580.

Kim, D. and Park, J. (2005) 'Analysis of flow structure over ogee-spillway in consideration of scale and roughness effects by using {CFD} model', *KSCE Journal of Civil Engineering*, 9(2), pp. 161–169. Available at: <http://dx.doi.org/10.1007/BF02829067>.

Lesleighter, E., McPherson, B., Riddette, K. and Williams, J. (2008) 'Modelling Procedures used for the Spillway Upgrade for Lake Manchester Dam', *ANCOLD Proceedings of Technical Groups: Dams and Water for the Future*, 1920.

Li, S., Cain, S., Wosnik, M., Miller, C., Kocahan, H. and Wyckoff, R. (2011) 'Numerical Modeling of Probable Maximum Flood Flowing through a System of Spillways', *Journal of Hydraulic Engineering*, 137(1), pp. 66–74. doi: 10.1061/(ASCE)HY.1943-7900.0000279.

Menter, F. R. (1994) 'Two-equation eddy-viscosity turbulence models for engineering applications', *AIAA Journal*. American Institute of Aeronautics and Astronautics, 32(8), pp. 1598–1605. doi: 10.2514/3.12149.

Morales, V., Tokyay, T. and Garcia, M. (2012) 'Numerical modelling of ogee crest spillway and tainter gate structure of a diversion dam on Canar River, Ecuador', *International conference on Water Resources CMWR 2012*, pp. 1–9.

Mu, Z., Zhang, Z. and Zhao, T. (2012) 'Numerical simulation of 3-D flow field of spillway based on VOF method', *Procedia Engineering*, 28(2011), pp. 808–812. doi: 10.1016/j.proeng.2012.01.814.

Nichols, B. D. and Hirt, C. W. (1975) ‘Methods for calculating multi-dimensional, transient, free surface flows past bodies’, in *Proceedings of the 1st International Conference on Ship Hydrodynamics*, pp. 253–277.

Nikuradse, J. (1932) *Gesetzmässigkeiten der turbulenten Stromung in glatten Rohren: aus dem Kaiser Wilhelm-Institut für Stromungsforschung Gottingen*. VDI Verlag GMBH (VDI Forschungsheft). Available at: <https://books.google.com.tr/books?id=PSpMnQEACAAJ>.

Parsaie, A., Haghiabi, A. H. and Moradinejad, A. (2015) ‘CFD modeling of flow pattern in spillway’s approach channel’, *Sustainable Water Resources Management*. Springer International Publishing, 1(3), pp. 245–251. doi: 10.1007/s40899-015-0020-9.

Rad, I. N. (2016) ‘Application of Numerical Methods in Design of Hydraulic Structures’, *Communications on Advanced Computational Science with Applications*, 2016(1), pp. 1–15. doi: 10.5899/2016/cacsa-00050.

Rahimzadeh, H., Maghsoodi, R., Sarkardeh, H. and Tavakkol, S. (2012) ‘Simulating flow over circular spillways by using different turbulence models’, *Engineering Applications of Computational Fluid Mechanics*, 6(1), pp. 100–109. doi: 10.1080/19942060.2012.11015406.

RECLAMATION, U. B. O. (1955) ‘Research studies on stilling basins, energy dissipators and associated appurtenances’, *Hydraulic Laboratory Report (USBR), no. HYD, 399*, pp. 393–438.

RECLAMATION, U. B. O. (2015) ‘VI-3 . Cavitation Damage Induced Failure of Spillways’, pp. 1–16.

Savage, B. M. and Johnson, M. C. (2001) ‘Flow over ogee spillway: Physical and numerical model case study’, *Journal of Hydraulic Engineering*, 127(8), pp. 640–649. doi: 10.1061/(ASCE)0733-9429(2001)127:8(640).

Sung-Duk, K., Lee, H.-J. and An, S.-D. (2010) ‘Improvement of hydraulic stability for spillway using CFD model’, *International Journal of the Physical Sciences*, 5(6)(June), pp. 774–780. Available at: <http://www.academicjournals.org/journal/IJPS/article-abstract/C1AE0AA26964>.

U S Army Corps Of Engineers (1992) ‘Hydraulic Design of Spillways’, *Design*, (EM 1110-2-1603), p. 170.

Valero, D., Bung, D., Crookston, B. M. and Matos, J. (2016) ‘Numerical investigation of USBR type III stilling basin performance downstream of smooth and stepped spillways’, *6th International Symposium on Hydraulic Structures*, 3406281608, pp. 652–663. doi: 10.15142/T340628160853.

Web-1 (2012) *Butterley Spillway – West Yorkshire, UK*. Available at: <https://forums.autodesk.com/autodesk/attachments/autodesk/66/242671/2/Butterley-6148375.jpg>.

Web-2 (2013) *Cefni Dam – Anglesey, UK*. Available at: <https://geotopoi.files.wordpress.com/2013/01/llyn-cefni-20130126-11-cefni-dam.jpg>.

Web-3 (2011) *Elkwater Fork Dam – West Virginia, USA*. Available at: https://www.nrcs.usda.gov/Internet/FSE_MEDIA/nrcs144p2_071092.jpg.